1   # An antisense RNA capable of modulating the
2   # expression of the tumor suppressor microRNA-34a
3

4   **Jason T. Serviss[1]*, Felix Clemens Richter[1,2], Jimmy Van den Eynden[3],**
5   **Nathanael Andrews[1], Miranda Houtman[1,4], Mattias Vesterlund[1], Laura**
6   **Schwarzmueller[1,5], Per Johnsson[6,7], Erik Larsson[3], Dan Grandér[1] †, Katja**
7   **Pokrovskaia Tamm[1]**
8

9   [1] Department of Oncology and Pathology, Karolinska Institutet, Stockholm, Sweden, SE-
10 17177
11 [2] Kennedy Institute of Rheumatology, University of Oxford, Roosevelt Drive, Oxford OX3 7FY,
12 UK
13 [3] Department of Medical Biochemistry and Cell Biology, Institute of Biomedicine, The
14 Sahlgrenska Academy, University of Gothenburg, SE-405 30 Gothenburg, Sweden
15 [4] Rheumatology Unit, Department of Medicine, Karolinska University Hospital, Solna,
16 Karolinska Institutet, Stockholm, Sweden
17 [5] Laboratory for Experimental Oncology and Radiobiology (LEXOR), Center for Experimental
18 Molecular Medicine (CEMM), Academic Medical Center, Amsterdam, The Netherlands
19 [6] Ludwig Institute for Cancer Research, Stockholm, Sweden
20 [7] Department of Cell and Molecular Biology, Karolinska Institutet, Stockholm, Sweden
21
22

23 *** Correspondence:**
24 Jason T. Serviss jason.serviss@ki.se
25
26

27 ## Abstract

28 The microRNA-34a is a well-studied tumor suppressor microRNA (miRNA)

29 and a direct downstream target of TP53 with roles in several pathways

30 associated with oncogenesis, such as proliferation, cellular growth, and

31 differentiation. Due to its broad tumor suppressive activity, it is not surprising

32 that *miR34a* expression is altered in a wide variety of solid tumors and

33 hematological malignancies. However, the mechanisms by which *miR34a* is

34 regulated in these cancers is largely unknown. In this study, we find that a

35 long non-coding RNA transcribed antisense to the *miR34a* host gene, is

36 critical for *miR34a* expression and mediation of its cellular functions in multiple

37 types of human cancer. We name this long non-coding RNA *lncTAM34a*, and

38 characterize its ability to facilitate *miR34a* expression under different types of

39 cellular stress in both *TP53* deficient and wild type settings.

Introduction

40

41 In recent years advances in functional genomics have revolutionized our

42 understanding of the human genome. Evidence now points to the fact that

43 approximately 75% of the genome is transcribed but only ~1.2% of this is

44 responsible for encoding proteins (International Human Genome Sequencing

45 Consortium 2004, Djebali et al. 2012). Of these recently identified elements,

46 long non-coding (lnc) RNAs are defined as transcripts exceeding 200 base

47 pairs (bp) in length with a lack of a functional open reading frame. Some

48 lncRNAs are dually classified as antisense (as) RNAs that are expressed from

49 the same locus as a sense transcript in the opposite orientation. Current

50 estimates using high-throughput transcriptome sequencing, indicate that up to

51 20-40% of the approximately 20,000 protein-coding genes exhibit antisense

52 transcription (Chen et al. 2004, Katayama et al. 2005, Ozsolak et al. 2010).

53 Systematic large-scale studies have shown aberrant expression of asRNAs to

54 be associated with tumorigenesis (Balbin et al. 2015) and, although

55 characterization of several of these has identified asRNA-mediated regulation

56 of multiple well known tumorigenic factors (Yap et al. 2010, Johnsson et al.

57 2013), the vast majority of potential tumor-associated lncRNAs have not yet

58 been characterized. The known mechanisms by which asRNAs accomplish

59 their regulatory functions are diverse, and include recruitment of chromatin

60 modifying factors (Rinn et al. 2007, Johnsson et al. 2013), acting as

61 microRNA (miRNA) sponges (Memczak et al. 2013), and causing

62 transcriptional interference (Conley et al. 2012).

63

64 Responses to cellular stress, e.g. DNA damage, sustained oncogene

2

65 expression, and nutrient deprivation, are all tightly controlled cellular pathways

66 that are almost universally dysregulated in cancer. Cellular signaling, in

67 response to these types of stresses, often converges on the transcription

68 factor TP53 that regulates transcription of coding and non-coding downstream

69 targets. One important non-coding target of TP53 is the tumor suppressor

70 miRNA known as *miR34a* (Raver-Shapira et al. 2007).

71 Upon TP53 activation *miR34a* expression is increased allowing it to down-

72 regulate target genes involved in cellular pathways such as growth factor

73 signaling, apoptosis, differentiation, and cellular senescence (Lal et al. 2011,

74 Slabakova et al. 2017). Thus, *miR34a* is a crucial factor in mediating activated

75 TP53 response and, the fact that it is often deleted or down-regulated in

76 human cancers indicates, its tumor suppressive effect and makes it a valuable

77 prognostic marker (Cole et al. 2008, Gallardo et al. 2009, Zenz et al. 2009,

78 Cheng et al. 2010, Liu et al. 2011). Reduced *miR34a* transcription is mediated

79 via epigenetic regulation in many solid tumors, including colorectal-,

80 pancreatic-, and ovarian cancer (Vogt et al. 2011), as well as numerous types

81 of hematological malignancies (Chim et al. 2010). In addition, *miR34a* has

82 been shown to be transcriptionally regulated via TP53 homologs, TP63 and

83 TP73, other transcription factors, e.g. STAT3 and MYC, and, in addition, post-

84 transcriptionally through miRNA sponging by the NEAT1 lncRNA (Chang et al.

85 2008, Su et al. 2010, Agostini et al. 2011, Rokavec et al. 2015, Ding et al.

86 2017). Despite these findings, the mechanisms underlying *miR34a* regulation

87 in the context of oncogenesis have not yet been fully elucidated.

88

3

89   Studies across multiple cancer types have reported a decrease in oncogenic

90   phenotypes when *miR34a* expression is induced in a *TP53*-null background,

91   although endogenous mechanisms for achieving this have not yet been

92   discovered (Liu et al. 2011, Ahn et al. 2012, Yang et al. 2012, Stahlhut et al.

93   2015, Wang et al. 2015). In addition, previous reports from large-scale studies

94   interrogating global TP53-mediated regulation of lncRNAs have identified a

95   lncRNA (known as RP3-510D11.2 and LINC01759) originating in the

96   antisense orientation from the *miR34a* locus that is induced upon numerous

97   forms of cellular stress (Rashi-Elkeles et al. 2014, Hunten et al. 2015, Leveille

98   et al. 2015, Ashouri et al. 2016, Kim et al. 2017). Despite this, none of these

99   studies have functionally characterized this transcript, which we name *Long-*

100   *Non-Coding Transcriptional Activator of MiR34a* (lncTAM34a). In this study

101   we functionally characterize the *lncTAM34a* transcript, and find that it

102   positively regulates *miR34a* expression resulting in a decrease of several

103   tumorigenic phenotypes. Furthermore, we find that *lncTAM34a*-mediated up-

104   regulation of *miR34a* is sufficient to induce endogenous cellular mechanisms

105   counteracting several types of stress stimuli in a *TP53*-deficient background.

106   Finally, similar to the functional roles of antisense transcription at protein-

107   coding genes, we identify a rare example of an antisense RNA capable of

108   regulating a cancer-associated miRNA.

109

110   **Results**

111

112   ***lncTAM34a* is a broadly expressed non-coding transcript whose levels**
113   **correlate with *miR34a* expression**

114

115   *lncTAM34a* is transcribed in a "head-to-head" orientation with approximately

116   100 base pair overlap with the *miR34a* host gene (HG) (**Fig. 1a**). Due to the

4

117   fact that sense/antisense pairs can be both concordantly and discordantly

118   expressed, we sought to evaluate this relationship in the case of *miR34a* HG

119   and its asRNA. Using a diverse panel of cancer cell lines, we detected co-

120   expression of both the *miR34a* HG and *lncTAM34a* (**Fig. 1b**). We used cell

121   lines with a known *TP53* status in the panel due to previous reports

122   that *miR34a* and *lncTAM34a* are known downstream targets of TP53. These

123   results indicate that *miR34a* HG and *lncTAM34a* are co-expressed and that

124   their expression levels correlate with *TP53* status, with *TP53*$^{-/-}$ cells tending to

125   have decreased or undetectable expression of both transcripts.

126
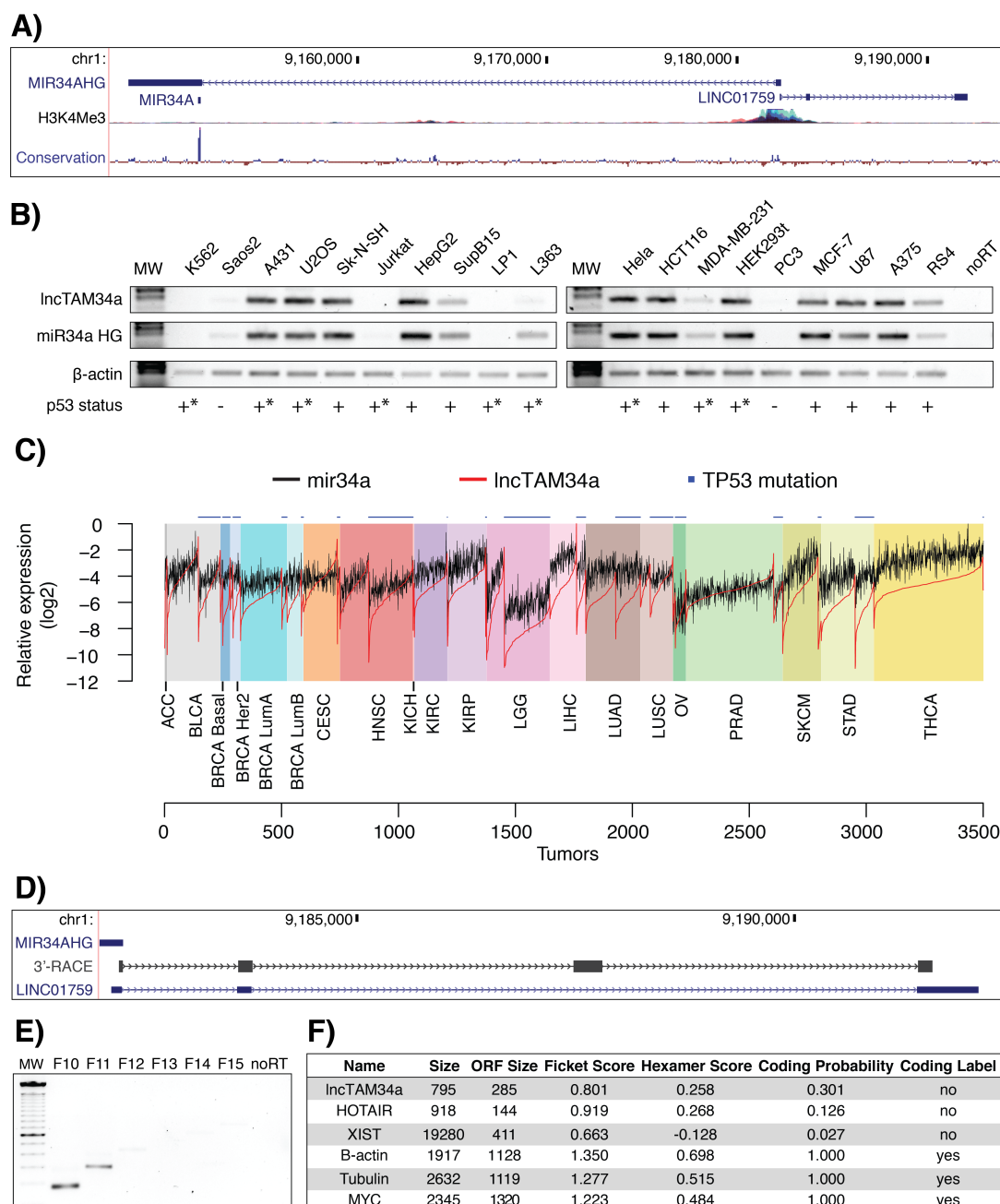
Figure 1: Characterization of the *lncTAM34a* transcript. A) Architecture of the *miR34a* locus (hg38, RefSeq) including *miR34a* HG, mature *miR34a*, and *lncTAM34a* (*LINC01759*). H3K4me3 ChIP-seq data, indicating the active promoter region, and conservation are also shown. **B)** Semi-quantitative PCR data from the screening of a panel of cancer cell lines. Wild type *TP53* is indicated with +, - indicates null, and +* represents either a non-null *TP53* mutation or wild-type *TP53* with mechanisms present that inhibit its function (e.g. SV40 large T antigen in HEK293T cells). **C)** TCGA correlation analysis. Expression was log2 normalized to the maximum expression value. Nonsynonymous *TP53* mutations are indicated on the top of the plot (cancer type abbreviation definitions and corresponding statistics are in Figure 1-Supplement 1). **D)** 3'-RACE sequencing results and the annotated *lncTAM34a* (*LINC01759*) are shown. **E)** Semi-quantitative PCR results from the primer walk assay (i.e. common reverse primer (exon 2) and forward primers (F10-F15) staggered upstream of *lncTAM34a*'s annotated start site) performed using HEK293T cells (Figure 1-Supplement 2a details primer placement) **F)** Coding potential analysis assessed via the Coding-potential Assessment Tool including *lncTAM34a*, two known non-coding RNAs (*HOTAIR* and *XIST*), and three protein-coding RNAs (β-actin, Tubulin, and *MYC*).

6

144   We next sought to analyze primary cancer samples to examine whether a

145   correlation between *lncTAM34a* and *miR34a* expression levels could be

146   identified. We utilized RNA sequencing data from The Cancer Genome Atlas

147   (TCGA) after stratifying patients by cancer type, *TP53* status, and, in the case

148   of breast cancer, cancer subtypes. The results indicate that *lncTAM34a*

149   and *miR34a* expression are strongly correlated in the vast majority of cancer

150   types examined, both in the presence and absence of wild-type *TP53* (**Fig.**

151   **1c, Figure 1-Figure Supplement 1a**). The results also further confirm that

152   the expression levels of both *miR34a* and *lncTAM34a* are significantly

153   reduced in patients with nonsynonymous *TP53* mutations (**Figure 1-Figure**

154   **Supplement 1b**).

155

156   Next, we aimed to gain a thorough understanding of *lncTAM34a*'s molecular

157   characteristics and cellular localization. To experimentally determine the 3'

158   termination site for the *lncTAM34a* transcript we performed 3' rapid

159   amplification of cDNA ends (RACE) using the U2OS osteosarcoma cell line

160   that exhibited high endogenous levels of *lncTAM34a* in the cell panel

161   screening. Sequencing the cloned cDNA indicated that the transcripts 3'

162   transcription termination site is 525 bp upstream of the *lncTAM34a* transcript's

163   annotated termination site (**Fig. 1d**). Next, we characterized the *lncTAM34a* 5'

164   transcription start site by carrying out a primer walk assay, i.e. a common

165   reverse primer was placed in exon 2 and forward primers were gradually

166   staggered upstream of *lncTAM34a*'s annotated start site (**Figure 1-Figure**

167   **Supplement 2a**). Our results indicated that the 5' start site for *lncTAM34a* is

168   in fact approximately 90 bp (F11 primer) to 220 bp (F12 primer) upstream of

169   the annotated start site (**Fig. 1e**). Polyadenylation status was evaluated via

170   cDNA synthesis with either random nanomers or oligo(DT) primers followed

171   by semi-quantitative PCR which showed that *lncTAM34a* is polyadenylated

172   although the unspliced form seems to only be present in a polyadenylation

173   negative state (**Figure 1-Figure Supplement 2b**). Furthermore, we

174   investigated the propensity of *lncTAM34a* to be alternatively spliced in U2OS

175   cells, using PCR cloning followed by sequencing and found that the transcript

176   is post-transcriptionally spliced to form multiple isoforms (**Figure 1-Figure**

177   **Supplement 2c**). In order to evaluate the subcellular localization of

178   *lncTAM34a*, we made use of RNA sequencing data from five cancer cell lines

179   included in the ENCODE (Encode Project Consortium 2012) project that had

180   been fractionated into cytosolic and nuclear fractions. The analysis revealed

181   that the *lncTAM34a* transcript primarily localizes to the nucleus with only a

182   minor fraction in the cytosol (**Figure 1-Figure Supplement 2d**).

183

184   Lastly, we utilized several approaches to evaluate the coding potential of

185   the *lncTAM34a* transcript. The Coding-Potential Assessment Tool is a

186   bioinformatics-based tool that uses a logistic regression model to evaluate

187   coding-potential by examining open reading frame (ORF) length, ORF

188   coverage, Fickett score, and hexamer score (Wang et al. 2013). Results

189   indicated that *lncTAM34a* has a similar low coding capacity to known non-

190   coding transcripts such as *HOTAIR* and *XIST* (Fig. 1F). We further confirmed

191   these results using the Coding-Potential Calculator that uses a support vector

192   machine-based classifier and accesses an alternate set of discriminatory

193   features (**Figure 1-Figure Supplement 2e**) (Kong et al. 2007). Finally, we

194   downloaded mass spectrometry spectra for 11 cancer cell lines (Geiger et al.

195   2012), 7 of which were also present in the cell line panel above (**Fig. 1b**), and

196   searched it against a database of human protein sequences which also

197   contained the 6 frame translation of *lncTAM34a*. However, we did not manage

198   to detect any peptides matching the sequence in any of the 11 cell lines.

199   Taken together our results indicate that *lncTAM34a* is not a coding transcript

200   and that it is not translated to any significant degree.

201

202   **TP53-mediated regulation of *lncTAM34a* expression**

203   *miR34a* is a known downstream target of TP53 and has been previously

204   shown to exhibit increased expression within multiple contexts of cellular

205   stress. Several global analyses of TP53-regulated lncRNAs have also shown

206   *lncTAM34a* to be induced upon TP53 activation (Rashi-Elkeles et al. 2014,

207   Hunten et al. 2015, Leveille et al. 2015, Ashouri et al. 2016, Kim et al. 2017).

208   To confirm these results in our biological systems, we treated HEK293T,

209   embryonic kidney cells, and HCT116, colorectal cancer cells, with the DNA

210   damaging agent doxorubicin to activate TP53. QPCR-mediated

211   measurements of both *miR34a* HG and *lncTAM34a* indicated that their

212   expression levels were increased in response to doxorubicin treatment in both

213   cell lines (**Fig. 2a**). To assess whether TP53 was responsible for the increase

214   in *lncTAM34a* expression upon DNA damage, we treated $TP53^{+/+}$ and $TP53^{-/-}$

215   HCT116 cells with increasing concentrations of doxorubicin and monitored the

216   expression of both *miR34a* HG and *lncTAM34a*. We observed a dose-

217   dependent increase in both *miR34a* HG and *lncTAM34a* expression levels

218   with increasing amounts of doxorubicin, revealing that these two transcripts

219   are co-regulated, although, this effect was largely abrogated in *TP53*^{-/-} cells

220   (**Fig. 2b**). These results indicate that TP53 activation increases *lncTAM34a*

221   expression upon DNA damage. Nevertheless, *TP53*^{-/-} cells also showed a

222   dose-dependent increase in both *miR34a* HG and *lncTAM34a*, suggesting

223   that additional factors, other than *TP53* are capable of initiating an increase in

224   expression of both of these transcripts upon DNA damage.

225
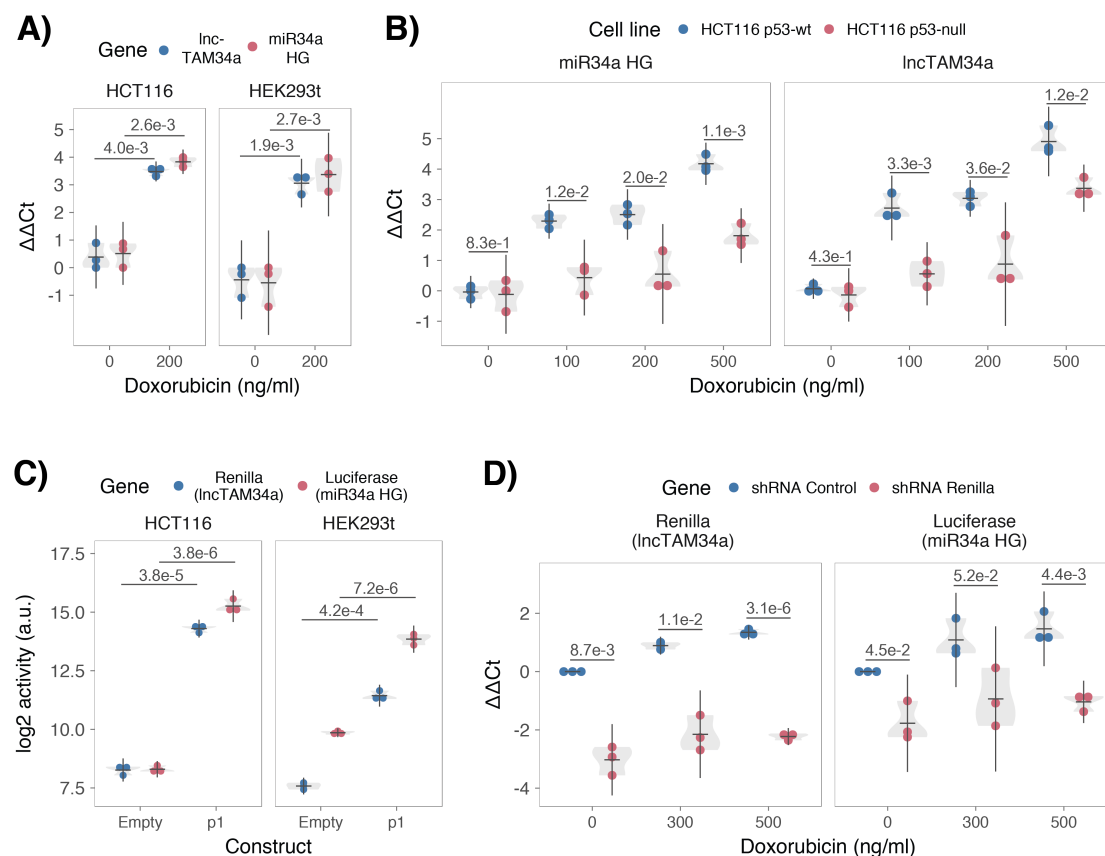
Figure 2: TP53-mediated regulation of the *miR34a* locus. A) Evaluating the effects of 24 hours of treatment with 200 ng/ml doxorubicin on *lncTAM34a* and *miR34a* HG in HCT116 and HEK293T cells.* **B)** Monitoring *miR34a* HG and *lncTAM34a* expression levels during 24 hours of doxorubicin treatment in $TP53^{+/+}$ and $TP53^{-/-}$ HCT116 cells.* **C)** Quantification of luciferase and renilla levels after transfection of HCT116 and HEK293T cells with the p1 construct (Figure 2-Supplement 2 contains a schematic representation of the p1 construct).* **D)** HCT116 cells were co-transfected with the p1 construct and shRNA renilla or shRNA control and subsequently treated with increasing doses of doxorubicin. 24 hours post-treatment, cells were harvested and renilla and luciferase levels were measured using QPCR.* *Individual points represent results from independent experiments and the gray shadow indicates the density of those points. Error bars show the 95% CI, black horizontal lines represent the mean, and *P* values are shown over long horizontal lines indicating the comparison tested. All experiments in Figure 2 were performed in biological triplicate.

11

240   The head-to-head orientation of *miR34a* HG and *lncTAM34a*, suggests that

241   transcription is initiated from a single promoter in a bi-directional manner (**Fig**

242   **1a**). To investigate whether *miR34a* HG and *lncTAM34a* are transcribed from

243   the same promoter as divergent transcripts, we cloned the previously reported

244   *miR34a* HG promoter, a ~300 bp region including the TP53 binding site and

245   the majority of the first exon of both transcripts, into a luciferase/renilla dual

246   reporter vector (**Figure 2-Figure Supplement 1a-b**) (Raver-Shapira et al.

247   2007). We hereafter refer to this construct as p1. Upon transfection of p1 into

248   HCT116 and HEK293T cell lines we observed increases in both luciferase

249   and renilla indicating that *miR34a* HG and *lncTAM34a* expression can be

250   regulated by a single promoter contained within the p1 construct (**Fig. 2c**).

251

252   ***lncTAM34a* facilitates *miR34a* induction in response to DNA damage**

253   We hypothesized that *lncTAM34a* may regulate *miR34a* HG levels and, in

254   addition, that the overlapping regions of the sense and antisense transcripts

255   may mediate this regulation. Knockdown of endogenous *lncTAM34a* is

256   complicated by its various isoforms (**Figure 1-Figure Supplement 2c**). For

257   this reason, we utilized the p1 construct to evaluate the regulatory role of

258   *lncTAM34a* on *miR34a* HG. Accordingly, we first co-transfected the p1

259   construct, containing the overlapping region of the two transcripts, and two

260   different short hairpin (sh) RNAs targeting renilla into HEK293T cells and

261   subsequently measured luciferase and renilla expression. The results

262   indicated that shRNA-mediated knock-down of the p1-renilla transcript

263   (corresponding   to *lncTAM34a*)   caused   p1-luciferase   (corresponding

264   to *miR34a* HG)   levels   to   concomitantly   decrease   (**Figure   2-Figure**

12

265   **Supplement 2**). The results suggest that *lncTAM34a* positively regulates

266   levels of *miR34a* HG and that the transcriptional product of *lncTAM34a* within

267   the p1 construct contributes to inducing a *miR34a* response. To further

268   support these conclusions and better understand the role of *lncTAM34a*

269   during TP53 activation, $TP53^{+/+}$ HCT116 cells were co-transfected with p1

270   and shRNA renilla (2.1) and subsequently treated with increasing doses of

271   doxorubicin. Again, the results showed a concomitant reduction in luciferase

272   levels upon knock-down of p1-renilla i.e. the *lncTAM34a* corresponding

273   segment of the p1 transcript (**Fig. 2d**). Furthermore, the results showed that in

274   the absence of p1-renilla the expected induction of p1-luciferase in response

275   to TP53 activation by DNA damage is abrogated. Collectively these results

276   indicate that *lncTAM34a* positively regulates *miR34a* expression and

277   furthermore, suggests that it is crucial for an appropriate TP53-

278   mediated *miR34a* response to DNA damage.

279

280   ***lncTAM34a* can regulate *miR34a* host gene independently of *TP53***

281   Despite the fact that TP53 regulates *miR34a* HG and *lncTAM34a* expression,

282   our results showed that other factors are also able to regulate this locus (**Fig.**

283   **2b**). Utilizing a lentiviral system, we stably over-expressed the *lncTAM34a*

284   transcript in three *TP53*-null cell lines, PC3 (prostate cancer), Saos2

285   (osteogenic sarcoma), and Skov3 (ovarian adenocarcinoma). We first

286   analyzed the levels of *lncTAM34a* in these stable cell lines, compared to

287   HEK293T cells, which have high endogenous levels of *lncTAM34a*. On

288   average, the over-expression was approximately 30-fold higher in the over-

289   expression cell lines than in HEK293T cells, roughly corresponding to

13

290   physiologically relevant levels in cells encountering a stress stimulus, such as

291   DNA damage (**Figure 3-Figure Supplement 1**). Analysis of *miR34a* levels in

292   the *lncTAM34a* over-expressing cell lines showed that this over-expression

293   resulted in a concomitant increase in the expression of *miR34a* in all three cell

294   lines (**Fig. 3a**). These results indicate that, in the absence of

295   *TP53*, *miR34a* expression may be rescued by activating *lncTAM34a*

296   expression.
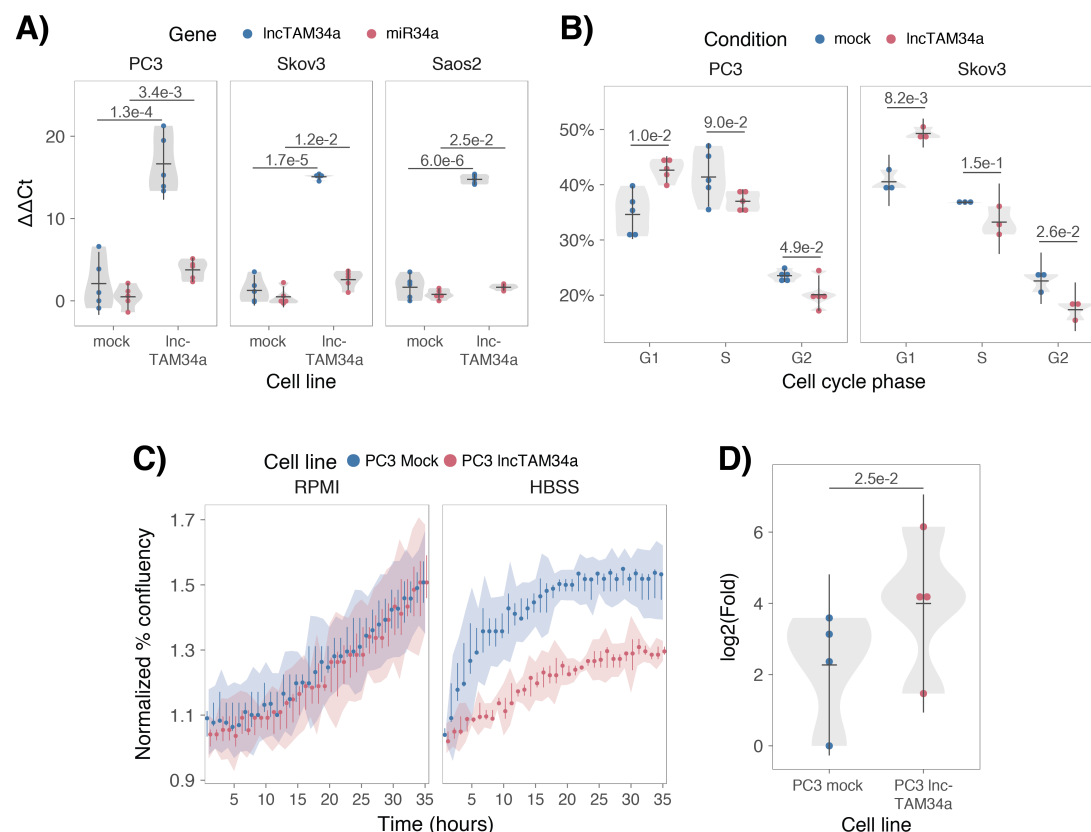
Figure 3: *lncTAM34a* **positively regulates** *miR34a* **and its associated phenotypes. A)** QPCR-mediated quantification of *miR34a* expression in cell lines stably over-expressing *lncTAM34a*.* **B)** Cell cycle analysis comparing stably over-expressing *lncTAM34a* cell lines to the respective mock control.* **C)** Analysis of cellular growth over time in *lncTAM34a* over-expressing PC3 cells. Points represent the median from 3 independent experiments, the colored shadows indicate the 95% confidence interval, and vertical lines show the minimum and maximum values obtained from the three experiments. **D)** Differential phosphorylated polymerase II binding in *lncTAM34a* over-expressing PC3 cells.* *Individual points represent results from independent experiments and the gray shadow indicates the density of those points. Error bars show the 95% CI, black horizontal lines represent the mean, and *P* values are shown over long horizontal lines indicating the comparison tested.

309   *miR34a* has been previously shown to regulate cell cycle progression, with

310   *miR34a* induction causing G1 arrest (Raver-Shapira et al. 2007, Tarasov et al.

311   2007). Cell cycle analysis via determination of DNA content showed a

312   significant increase in G1 phase cells and a concomitant decrease in G2

313   phase cells in the PC3 and Skov3 *lncTAM34a* over-expressing cell lines,

314   indicating G1 arrest (**Fig. 3b**). The effects of *miR34a* on the cell cycle are

315   mediated by its ability to target cell cycle regulators such as cyclin D1

316   (*CCND1*) *(Sun et al. 2008)*. Quantification of both *CCND1* RNA expression

317   (**Figure 3-Figure Supplement 2a**) and protein levels (**Figure 3-Figure**

318   **Supplement 2b**) in the PC3 *lncTAM34a* over-expressing cell line showed a

319   significant decrease of *CCND1* levels compared to the mock control.

320   Collectively, these results indicate that *lncTAM34a*-mediated induction of

321   *miR34a* is sufficient to result in the corresponding *miR34a*-directed effects on

322   cell cycle.

323

324   *miR34a* is also a well-known inhibitor of cellular growth via its ability to

325   negatively regulate growth factor signaling. Furthermore, starvation has been

326   shown to induce *miR34a* expression causing inactivation of numerous pro-

327   survival growth factors *(Lal et al. 2011)*. We further interrogated the effects

328   of *lncTAM34a* over-expression by monitoring the growth of the PC3 stable cell

329   lines in both normal and starvation conditions via confluency measurements

330   over a 35-hour period. Under normal growth conditions there is a small but

331   significant reduction (P = 3.0e-8; linear regression, **Fig. 3c**) in confluency in

332   the *lncTAM34a* over-expressing cell lines compared to mock control.

333   However, these effects on cell growth are drastically increased in starvation

16

334   conditions (P = 9.5e-67; linear regression; **Fig. 3c**). This is in agreement with

335   our previous results, and suggests that *lncTAM34a*-mediated increases

336   in *miR34a* expression are crucial under conditions of stress and necessary for

337   the initiation of an appropriate cellular response. In summary, we find that

338   over-expression of *lncTAM34a* is sufficient to increase *miR34a* expression

339   and gives rise to known phenotypes observed upon induction of *miR34a*.

340

341   ***lncTAM34a* transcriptionally activates *miR34a* host gene**

342   Antisense RNAs have been reported to mediate their effects both via

343   transcriptional and post-transcriptional mechanisms. Due to the fact that

344   *miR34a* expression is undetected in wild type PC3 cells (**Fig. 1b**) but, upon

345   over-expression of *lncTAM34a*, increases to detectable levels, we

346   hypothesized that *lncTAM34a* is capable of regulating *miR34a* expression via

347   a transcriptional mechanism. To ascertain if this is actually the case, we

348   performed chromatin immunoprecipitation (ChIP) for phosphorylated

349   polymerase II (polII) at the *miR34a* HG promoter in both *lncTAM34a* over-

350   expressing and mock control cell lines. Our results indicated a clear increase

351   in phosphorylated polII binding at the *miR34a* promoter upon *lncTAM34a*

352   over-expression indicating the ability of *lncTAM34a* to transcriptionally

353   regulate *miR34a* levels (**Fig. 3d**).

354

17
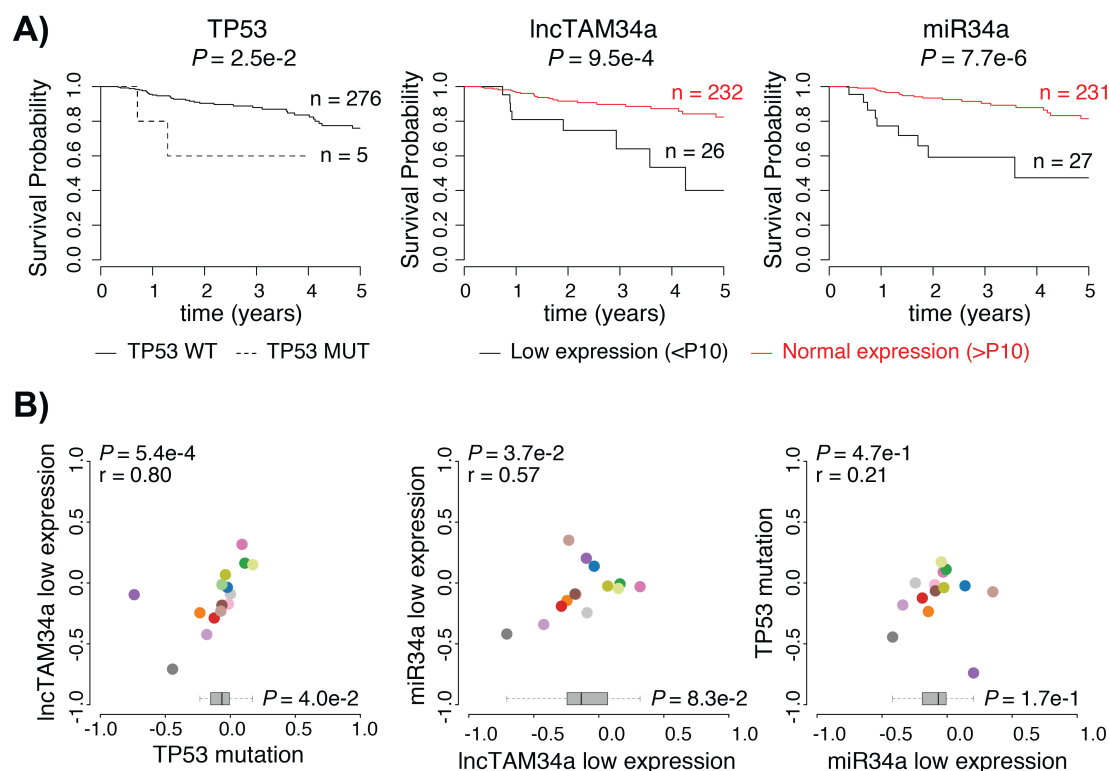
Figure 4: Survival analysis in TCGA cancers. A) Kaplan-Meier survival curves comparing the effects of *TP53*-mutated samples (left), low *lncTAM34a* expression (middle) and low *miR34a* expression (right) to control samples in papillary kidney cancer (results for other cancers in Figure 4-Supplement 1). Middle and Right panel include only TP53 wild type patients where RNAseq data exists. **B)** Correlation analysis between the effects on the 5-year survival probability of *TP53*-mutated samples, low *lncTAM34a* expression, and low *miR34a* expression as indicated. For each variable the 5-year survival probability was compared to the control group (negative values indicate lower survival, positive values indicate higher survival). Spearman correlation coefficients are given on the top left of each plot. Each dot indicates one cancer type (see Fig. 1c for legend). Boxplots on the bottom summarize the effects for the parameter on the x-axis, with indication of *P* values, as calculated using paired Wilcoxon signed rank test. Low expression was defined as *TP53* non-mutated samples having expression values in the bottom 10th percentile.

368
369 **Low *lncTAM34a* expression levels are associated with decreased**
370 **survival**
371
372 As *TP53* mutations and low expression of *miR34a* have been associated with

373 worse prognosis in cancer, we compared survival rates of samples with low

374 expression of *lncTAM34a* (bottom 10th percentile) to control samples in 17

375 cancer types from TCGA (**Figure 4-Supplement 1**) (Gallardo et al. 2009,

376 Zenz et al. 2009, Liu et al. 2011). To correct for the effect of *TP53* mutations

377 we focused on non-*TP53* mutated samples, and noted a worse survival for the

378 low expression group in several cancers. This effect was most pronounced in

379 papillary kidney cancer (unadjusted *P*=0.00095; **Fig. 4a**). By systematically

380 comparing 5-year survival probabilities between the low expression group and

381 the control group for each cancer we found a median reduction of 5-year

382 survival probability of 9.6% (*P*=0.083; Wilcoxon signed rank test; **Fig. 4b**).

383 Furthermore, we found that *lncTAM34a* expression showed similar patterns in

384 terms of direction and strength of association with 5-year survival probability

385 as *miR34a* expression (r=0.57, *P*=0.037) and TP53 mutations (r=0.80,

386 *P*=0.00054) across the different cancer types (**Fig. 4b**). Although these results

387 do not implicate any causal relationship, they do indicate a striking similarity

388 between the association of worse prognosis and *TP53* mutations, low

389 *miR34a*, and low *lncTAM34a* expression.

19

390
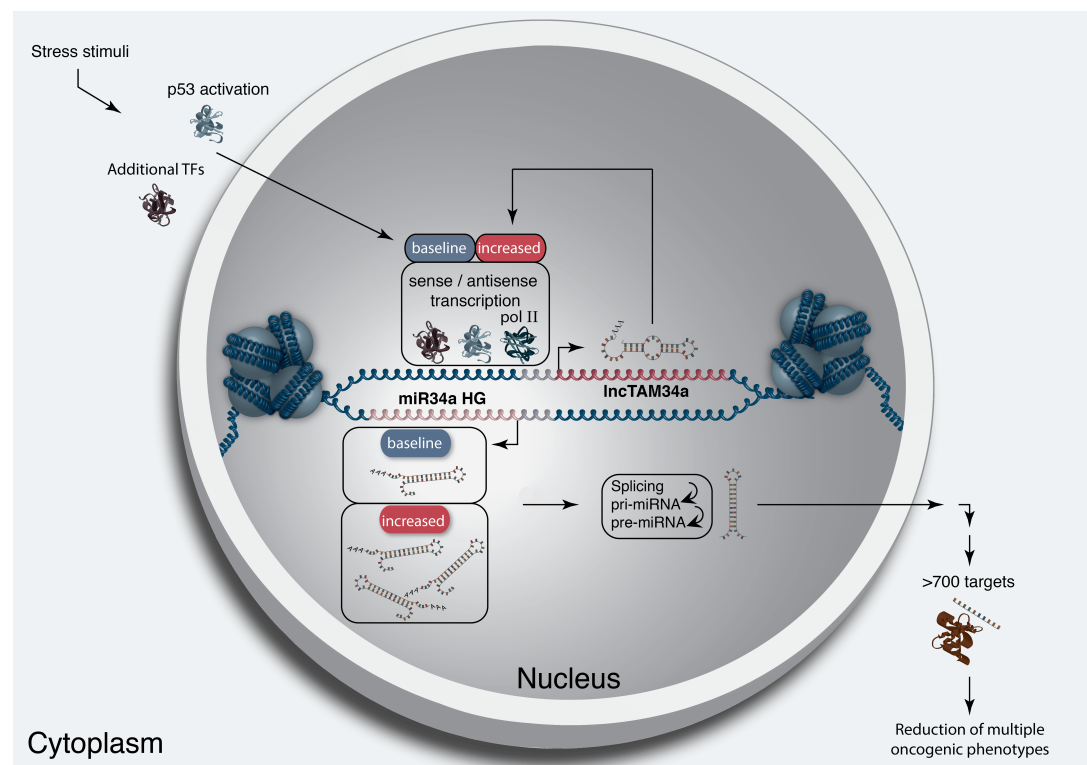
Figure 5: A graphical summary of the proposed *lncTAM34a* function. Stress stimuli, originating in the cytoplasm or nucleus, activate TP53 as well as additional factors. These factors then bind to the *miR34a* promoter and drive baseline transcription levels of the sense and antisense strands. *lncTAM34a* serves to further increase *miR34a* HG transcription levels resulting in enrichment of polymerase II at the *miR34a* promoter and a positive feed-forward loop. *miR34a* HG then, in turn, is spliced and processed in multiple steps before the mature *miR34a* binds to the RISC complex allowing it to repress its targets and exert its tumor suppressive effects.

20

Discussion

Multiple studies have previously shown asRNAs to be crucial for the appropriate regulation of cancer-associated protein-coding genes and that their dysregulation can lead to perturbance of tumor suppressive and oncogenic pathways, as well as, cancer-related phenotypes (Yu et al. 2008, Yap et al. 2010, Serviss et al. 2014, Balbin et al. 2015). Here we show that asRNAs are also capable of regulating cancer-associated miRNAs resulting in similar consequences as protein-coding gene dysregulation (**Fig. 4**). Interestingly, we show that, both in the presence and absence of *TP53*, *lncTAM34a* provides an additional regulatory level to control *miR34a* expression in both homeostasis and upon encountering various forms of cellular stress. Furthermore, we find that *lncTAM34a*-mediated increase in *miR34a* expression is sufficient to drive the appropriate cellular responses to these stress stimuli (**Fig. 2d and Fig. 3c**). Previous studies have exploited various molecular biology methods to up-regulate *miR34a* expression in cells lacking wild type *TP53* (Liu et al. 2011, Ahn et al. 2012, Yang et al. 2012, Stahlhut et al. 2015, Wang et al. 2015). In this study, we demonstrate a novel, endogenous mechanism of *miR34a* regulation that has similar phenotypic outcomes as has been previously shown for *miR34a* induction in a *TP53* deficient background.

In agreement with previous studies, we demonstrate that upon encountering various types of cellular stress, TP53 in concert with additional factors initiates transcription at the *miR34a* locus, thus increasing the levels of *lncTAM34a* and *miR34a* (Rashi-Elkeles et al. 2014, Hunten et al. 2015, Leveille et al.

21

424 2015, Ashouri et al. 2016, Kim et al. 2017). We found that over-expression of

425 *lncTAM34a* leads to recruitment of polII to the *miR34a* promoter and

426 hypothesize that *lncTAM34a* may provide positive feedback for *miR34a*

427 expression whereby it serves as a scaffold for the recruitment of additional

428 factors that facilitate polII-mediated transcription. In this manner, *miR34a*

429 expression is induced, driving a shift towards a reduction in growth factor

430 signaling, senescence, and in some cases apoptosis. On the other hand, in

431 cells without functional TP53, other factors, which typically act independently

432 or in concert with TP53, may initiate transcription of the *miR34a* locus. Due to

433 the fact that *lncTAM34a* can alter *miR34a* expression in these cells, we

434 suggest that it is interacting with one of these additional factors, possibly

435 recruiting it to the *miR34a* locus in order to drive *miR34a* transcription, similar

436 to mechanisms described for other lncRNAs (Hung et al. 2011, Ng et al. 2012,

437 Ng et al. 2013). The head-to-head orientation of the *miR34a* HG and

438 *lncTAM34a* causes sequence complementarity between the RNA and the

439 promoter DNA, making targeting by direct binding an attractive mechanism.

440 Previous reports have also illustrated the ability of asRNAs to form hybrid

441 DNA:RNA R-loops and, thus, facilitate an open chromatin structure and the

442 transcription of the sense gene (Boque-Sastre et al. 2015). The fact that the

443 p1 construct only contains a small portion (~300 bp) of the *lncTAM34a*

444 transcript indicates that this portion is sufficient to give rise to at least a partial

445 *miR34a* inducing response and therefore, that *lncTAM34a* may be able to

446 facilitate *miR34a* expression independent of additional factors (**Fig 2d, Figure**

447 **2-Figure Supplement 2a**). Nevertheless, further work will need to be

448 performed to explore the mechanism whereby *lncTAM34a* regulates *miR34a*

22

449   gene expression.

450

451   An antisense transcript arising from the *miR34a* locus, *Lnc34a*, has been

452   previously reported to negatively regulate the expression of *miR34a* (Wang et

453   al. 2016). Although the *Lnc34a* and *lncTAM34a* transcripts share some

454   sequence similarity, we believe them to be separate RNAs that are,

455   potentially, different isoforms of the same gene. We utilized CAGE and

456   RNAseq data from the ENCODE project to evaluate the presence of

457   *lncTAM34a* and *Lnc34a* in 28 and 36 commonly used cancer cell lines,

458   respectively. Although the results show the presence of *lncTAM34a* in these

459   cell lines, we find no evidence for *Lnc34a* transcription (**Supplementary**

460   **Document 1)**. These results are in line with the findings of Wang et al.

461   indicating that *Lnc34a* is highly expressed in colon cancer stem cell spheres

462   compared to all other cell types used in their study and may not be broadly

463   expressed in other tissues or tumor types. The fact that *lncTAM34a* and

464   *Lnc34a* would appear to have opposing roles in their regulation of *miR34a*,

465   further underlines the complexity of the regulation at this locus.

466

467   Clinical trials utilizing *miR34a* replacement therapy have previously been

468   conducted but, disappointingly, were terminated after adverse side effects of

469   an immunological nature were observed in several of the patients (Slabakova

470   et al. 2017). Although it is not presently clear if these side effects were caused

471   by *miR34a* or the liposomal carrier used to deliver the miRNA, the multitude of

472   evidence indicating *miR34a*'s crucial role in oncogenesis still makes its

473   therapeutic induction an interesting strategy and needs further investigation.

474   Our results indicate an association between survival probability and low

475   *lncTAM34a* expression making it an attractive candidate for controlled

476   preclinical studies. Due to the *lncTAM34a*-mediated positive feedback on

477   *miR34a* expression, initiation of this feedback mechanism may provide a

478   sustained *miR34a* induction in a relatively more robust manner than *miR34a*

479   replacement alone. In summary, our results have identified *lncTAM34a* as a

480   vital component in the regulation of *miR34a* and its particular importance in

481   typical examples of cellular stress encountered in cancer. On a broader level,

482   the conclusions drawn in this study provide an example of asRNA-mediated

483   regulation of a clinically relevant cancer-associated miRNA and contribute to

484   fundamental knowledge concerning *miR34a* regulation.

485

486   **Materials and Methods**

487   **Cell Culture**

488   All cell lines were cultured at 5% CO_2 and 37°C with HEK293T, Saos2, and

489   Skov3 cells cultured in DMEM high glucose (GE Healthcare Life Sciences,

490   Hyclone, Amersham. UK, Cat# SH30081), HCT116 and U2OS cells in

491   McCoy's 5a (ThermoFisher Scientific, Pittsburgh, MA, USA. Cat# SH30200),

492   and PC3 cells in RPMI (GE Healthcare Life Sciences, Hyclone, Cat#

493   SH3009602) and 2 mM L-glutamine (GE Healthcare Life Sciences, Hyclone,

494   Cat# SH3003402). All growth mediums were supplemented with 10% heat-

495   inactivated FBS (ThermoFisher Scientific, Gibco, Cat# 12657029) and 50

496   µg/ml of streptomycin (ThermoFisher Scientific, Gibco, Cat# 15140122) and

497   50 µg/ml of penicillin (ThermoFisher Scientific, Gibco, Cat# 15140122). All cell

498   lines were purchased from ATCC, tested negative for mycoplasma, and their

499   identity was verified via STR profiling.

500
501   **Bioinformatics, Data Availability, and Statistical Testing**

502   The USCS genome browser (Kent et al. 2002) was utilized for the

503   bioinformatic evaluation of antisense transcription utilizing the RefSeq

504   (O'Leary et al. 2016) gene annotation track.

505

506   All raw experimental data, code used for analysis, and supplementary

507   methods are available for review at (Serviss 2017) and are provided as an R

508   package. All analysis took place using the R statistical programming language

509   (Team 2017) using external packages that are documented in the package

510   associated with this article (Wilkins , Chang 2014, Wickham 2014, Therneau

511   2015, Wickham 2016, Allaire et al. 2017, Arnold 2017, Wickham 2017,

512   Wickham 2017, Wickham 2017, Xiao 2017, Xie 2017). The package facilitates

513   replication of the operating system and package versions used for the original

514   analysis, reproduction of each individual figure and figure supplement

515   included in the article, and easy review of the code used for all steps of the

516   analysis, from raw-data to figure.

517

518   The significance threshold (alpha) in this study was set to 0.05. Statistical

519   testing was performed using an unpaired two sample Student's t-test unless

520   otherwise specified.

521

522   **Coding Potential**

523   Protein-coding capacity was evaluated using the Coding-potential

524   Assessment Tool (Wang et al. 2013) and Coding-potential Calculator (Kong et

25

525   al. 2007) with default settings. Transcript sequences for use with Coding-

526   potential Assessment Tool were downloaded from the UCSC genome

527   browser   using   the   Ensembl

528   accessions: *HOTAIR* (ENST00000455246), *XIST* (ENST00000429829),   β-

529   actin   (ENST00000331789),   Tubulin   (ENST00000427480),

530   and *MYC* (ENST00000377970). Transcript sequences for use with Coding-

531   potential Calculator were downloaded from the UCSC genome browser using

532   the following IDs: *HOTAIR* (uc031qho.1), β-actin (uc003soq.4).

533

534   **Peptide identification in MS/MS spectra**

535   Orbitrap raw MS/MS files for 11 human cell lines were downloaded from the

536   PRIDE repository (PXD002395; (Geiger et al. 2012)) converted to mzML

537   format using msConvert from the ProteoWizard tool suite (Holman et al.

538   2014). Spectra were then searched using MSGF+ (v10072) (Kim et al. 2014)

539   and Percolator (v2.08) (Granholm et al. 2014). All searches were done

540   against the human protein subset of Ensembl 75 in the Galaxy platform

541   (Boekel et al. 2015) supplemented with the 6 frame translation of both the

542   annotated (LOC102724571; hg38) and PCR cloned sequence of *lncTAM34a*

543   (supplementary data; (Serviss 2017)). MSGF+ settings included precursor

544   mass tolerance of 10 ppm, fully-tryptic peptides, maximum peptide length of

545   50 amino acids and a maximum charge of 6. Fixed modification was

546   carbamidomethylation on cysteine residues; a variable modification was used

547   for oxidation on methionine residues. Peptide Spectral Matches found at 1%

548   FDR (false discovery rate) were used to infer peptide identities. The output

549   from all searches are available in (Serviss 2017).

550

shRNAs

552 shRNA-expressing constructs were cloned into the U6M2 construct using the

553 BglII and KpnI restriction sites as previously described (Amarzguioui et al.

554 2005). shRNA constructs were transfected using Lipofectamine 2000 or 3000

555 (ThermoFisher Scientific, Cat# 12566014 and L3000015). The sequences

556 targeting renilla is as follows: shRenilla 1.1 (AAT ACA CCG CGC TAC TGG

557 C), shRenilla 2.1 (TAA CGG GAT TTC ACG AGG C).

558

Bi-directional Promoter Cloning

560 The overlapping region (p1) corresponds with the sequence previously

561 published as the TP53 binding site in (Raver-Shapira et al. 2007) which we

562 synthesized, cloned into the pLucRluc construct (Polson et al. 2011), and

563 sequenced to verify its identity.

564

Promoter Activity

566 Cells were co-transfected with the p1 renilla/firefly bidirectional promoter

567 construct (Polson et al. 2011) and GFP by using Lipofectamine 2000 (Life

568 Technologies, Cat# 12566014). The expression of GFP and luminescence

569 was measured 24 h post transfection by using the Dual-Glo Luciferase Assay

570 System (Promega, Cat# E2920) and detected by the GloMax-Multi+ Detection

571 System (Promega, Cat# SA3030). The expression of luminescence was

572 normalized to GFP.

573

Generation of U6-expressed *lncTAM34a* Lentiviral Constructs

575　The U6 promoter was amplified from the U6M2 cloning plasmid (Amarzguioui

576　et al. 2005) and ligated into the Not1 restriction site of the pHIV7-IMPDH2

577　vector (Turner et al. 2012). *lncTAM34a* was PCR amplified and subsequently

578　cloned into the Nhe1 and Pac1 restriction sites in the pHIV7-IMPDH2-U6

579　plasmid.

580

581　**Lentiviral Particle production, infection, and selection**

582　Lentivirus production was performed as previously described in (Turner et al.

583　2012). Briefly, HEK293T cells were transfected with viral and expression

584　constructs using Lipofectamine 2000 (ThermoFisher Scientific, Cat#

585　12566014), after which viral supernatants were harvested 48 and 72 hours

586　post-transfection. Viral particles were concentrated using PEG-IT solution

587　(Systems Biosciences, Palo Alto, CA, USA. Cat# LV825A-1) according to the

588　manufacturer's recommendations. HEK293T cells were used for virus titration

589　and GFP expression was evaluated 72hrs post-infection via flow cytometry

590　(LSRII, BD Biosciences, San Jose, CA, USA) after which TU/ml was

591　calculated.

592

593　Stable lines were generated by infecting cells with a multiplicity of infection of

594　1 and subsequently initiating 1-2 µM mycophenolic acid-based (Merck,

595　Kenilworth, NJ, USA. Cat# M5255) selection 48-72 hours post-infection. Cells

596　were expanded as the selection process was monitored via flow cytometry

597　analysis (LSRII, BD Biosciences) of GFP and selection was terminated once

598　> 90% of the cells were GFP positive. Quantification of *lncTAM34a* over-

599　expression and *miR34a* was performed in biological quintuplet for all cell

600   lines.

601

Western Blotting

603   Samples were lysed in 50 mM Tris-HCl (Sigma Aldrich, St. Louis, MO, USA.

604   Cat# T2663), pH 7.4, 1% NP-40 (Sigma Aldrich, Cat# I8896), 150 mM NaCl

605   (Sigma Aldrich, Cat# S5886), 1 mM EDTA (Promega, Madison, WI, USA.

606   Cat# V4231), 1% glycerol (Sigma Aldrich, Cat# G5516), 100 µM vanadate

607   (Sigma Aldrich, Cat# S6508), protease inhibitor cocktail (Roche Diagnostics,

608   Basel, Switzerland, Cat# 004693159001) and PhosSTOP (Roche

609   Diagnostics, Cat# 04906837001). Lysates were subjected to SDS-PAGE and

610   transferred to PVDF membranes. The proteins were detected by western blot

611   analysis by using an enhanced chemiluminescence system (Western

612   Lightning–ECL, PerkinElmer, Waltham, MA, USA. Cat# NEL103001EA).

613   Antibodies used were specific for CCND1 1:1000 (Cell Signaling, Danvers,

614   MA, USA. Cat# 2926), and GAPDH 1:5000 (Abcam, Cambridge, UK, Cat#

615   ab9485). All western blot quantifications were performed using ImageJ

616   (Schneider et al. 2012).

617

RNA Extraction and cDNA Synthesis

619   For downstream SYBR green applications, RNA was extracted using the

620   RNeasy mini kit (Qiagen, Venlo, Netherlands, Cat# 74106) and subsequently

621   treated with DNase (Ambion Turbo DNA-free, ThermoFisher Scientific, Cat#

622   AM1907). 500ng RNA was used for cDNA synthesis using MuMLV

623   (ThermoFisher Scientific, Cat# 28025013) and a 1:1 mix of oligo(dT) and

624   random nanomers.

625

626   For analysis of miRNA expression with Taqman, samples were isolated with

627   TRIzol reagent (ThermoFisher Scientific, Cat# 15596018) and further

628   processed with the miRNeasy kit (Qiagen, Cat# 74106). cDNA synthesis was

629   performed using the TaqMan MicroRNA Reverse Transcription Kit

630   (ThermoFisher Scientific, Cat# 4366597) using the corresponding oligos

631   according to the manufacturer's recommendations.

632

633   **QPCR and PCR**

634   PCR was performed using the KAPA2G Fast HotStart ReadyMix PCR Kit

635   (Kapa Biosystems, Wilmington, MA, USA, Cat# KK5601) with corresponding

636   primers. QPCR was carried out using KAPA 2G SYBRGreen (Kapa

637   Biosystems, Cat# KK4602) using the Applied Biosystems 7900HT machine

638   with the cycling conditions: 95 °C for 3 min, 95 °C for 3 s, 60 °C for 30 s.

639

640   QPCR for miRNA expression analysis was performed according to the primer

641   probe set manufacturers recommendations (ThermoFisher Scientific) and

642   using the TaqMan Universal PCR Master Mix (ThermoFisher Scientific, Cat#

643   4304437) with the same cycling scheme as above. Primer and probe sets for

644   TaqMan were also purchased from ThermoFisher Scientific (Life

645   Technologies at time of purchase, TaqMan® MicroRNA Assay, hsa-miR-34a,

646   human, Cat# 4440887, Assay ID: 000426 and Control miRNA Assay, RNU48,

647   human, Cat# 4440887, Assay ID: 001006).

648

649   The ΔΔCt method was used to quantify gene expression. All QPCR-based

650   experiments were performed in at least technical duplicate. Primers for all

651   PCR-based experiments are listed in **Supplementary Document 2** and

652   arranged by figure.

653

654   **Cell Cycle Distribution**

655   Cells were washed in PBS and fixed in 4% paraformaldehyde at room

656   temperature overnight. Paraformaldehyde was removed, and cells were re-

657   suspended in 95% EtOH. The samples were then rehydrated in distilled

658   water, stained with DAPI and analyzed by flow cytometry on a LSRII (BD

659   Biosciences) machine. Resulting cell cycle phases were quantified using the

660   ModFit software (Verity Software House, Topsham, ME, USA). Experiments

661   were performed in biological quadruplet (PC3) or triplicate (Skov3). The log2

662   fraction of cell cycle phase was calculated for each replicate and a two

663   sample t-test was utilized for statistical testing.

664

665   **3' Rapid Amplification of cDNA Ends**

666   3'-RACE was performed as described as previously in (Johnsson et al. 2013).

667   Briefly, U2OS cell RNA was polyA-tailed using yeast polyA polymerase

668   (ThermoFisher Scientific, Cat# 74225Z25KU) after which cDNA was

669   synthesized using oligo(dT) primers. Nested-PCR was performed first using a

670   forward primer in *lncTAM34a* exon 1 and a tailed oligo(dT) primer followed by

671   a second PCR using an alternate *lncTAM34a* exon 1 primer and a reverse

672   primer binding to the tail of the previously used oligo(dT) primer. PCR

673   products were gel purified and cloned the Strata Clone Kit (Agilent

674   Technologies, Santa Clara, CA, USA. Cat# 240205), and sequenced.

675

676 **Chromatin Immunoprecipitation**

677 The ChIP was performed as previously described in (Johnsson et al. 2013)

678 with the following modifications. Cells were crosslinked in 1% formaldehyde

679 (Merck, Cat# 1040039025), quenched with 0.125M glycine (Sigma Aldrich,

680 Cat# G7126), and lysed in cell lysis buffer comprised of: 5mM PIPES (Sigma

681 Aldrich, Cat# 80635), 85mM KCL (Merck, Cat# 4936), 0.5% NP40 (Sigma

682 Aldrich, Cat# I8896), protease inhibitor (Roche Diagnostics, Cat#

683 004693159001). Samples were then sonicated in 50mM TRIS-HCL pH 8.0

684 (Sigma Aldrich, MO, USA, Cat# T2663) 10mM EDTA (Promega, WI, USA,

685 Cat# V4231), 1% SDS (ThermoFisher Scientific, Cat# AM9822), and protease

686 inhibitor (Roche Diagnostics, Cat# 004693159001) using a Bioruptor

687 Sonicator (Diagenode, Denville, NJ, USA). Samples were incubated over

688 night at 4°C with the polII antibody (Abcam, Cat# ab5095) and subsequently

689 pulled down with Salmon Sperm DNA/Protein A Agarose (Millipore, Cat# 16-

690 157) beads. DNA was eluted in an elution buffer of 1% SDS (ThermoFisher

691 Scientific, Cat# AM9822) 100mM NaHCO3 (Sigma Aldrich, Cat# 71631),

692 followed by reverse crosslinking, RNaseA (ThermoFisher Scientific, Cat#

693 1692412) and protease K (New England Biolabs, Ipswich, MA, USA, Cat#

694 P8107S) treatment. The DNA was eluted using Qiagen PCR purification kit

695 (Cat# 28106) and quantified via QPCR. QPCR was performed in technical

696 duplicate using the standard curve method and reported absolute values. The

697 fraction of input was subsequently calculated using the mean of the technical

698 replicates followed by calculating the fold over the control condition. Statistical

699 testing was performed using 4 biological replicates with the null hypothesis

700   that the true log2 fold change values were equal to zero.

701

Confluency Analysis

703   Cells were incubated in the Spark Multimode Microplate (Tecan, Männedorf,

704   Switzerland) reader for 48 hours at 37°C with 5% CO_2 in a humidity chamber

705   in either normal medium or HBSS (ThermoFisher Scientific, Cat# 14025092) .

706   Confluency was measured every hour using bright-field microscopy and the

707   percentage of confluency was reported via the plate reader's inbuilt algorithm.

708   Percentage of confluency was normalized to the control sample in each

709   condition (shown in figure) and then ranked to move the data to a linear scale.

710   Using the mean of the technical duplicates in three biological replicates, the

711   rank was then use to construct a linear model, of the dependency of the rank

712   on the time and cell lines variables for each growth condition. Reported *P*

713   values are derived from the t-test, testing the null hypothesis that the

714   coefficient estimate of the cell line variable is equal to 0.

715

Pharmacological Compounds

717   Doxorubicin was purchased from Teva (Petah Tikva, Israel, cat. nr. 021361).

718

Cellular Localization Analysis

720   Quantified RNAseq data from 11 cell lines from the GRCh38 assembly was

721   downloaded from the ENCODE project database and quantifications for

722   *lncTAM34a* (ENSG00000234546), GAPDH (ENSG00000111640), and

723   MALAT1 (ENSG00000251562) were extracted. Cell lines for which data was

724   downloaded include: A549, GM12878, HeLa-S3, HepG2, HT1080, K562

725 MCF-7, NCI-H460, SK-MEL-5, SK-N-DZ, SK-N-SH. Initial exploratory analysis

726 revealed that several cell lines should be removed from the analysis due to a)

727 a larger proportion of GAPDH in the nucleus than cytoplasm or b) variation of

728 *lncTAM34a* expression is too large to draw conclusions, or c) they have no or

729 low (<6 TPM) *lncTAM34a* expression. Furthermore, only polyadenylated

730 libraries were used in the final analysis, due to the fact that the cellular

731 compartment enrichment was improved in these samples. All analyzed genes

732 are reported to be polyadenylated. In addition, only samples with 2 biological

733 replicates were retained. For each cell type, gene, and biological replicate the

734 fraction of transcripts per million (TPM) in each cellular compartment was

735 calculated as the fraction of TPM in the specific compartment by the total

736 TPM. The mean and standard deviation for the fraction was subsequently

737 calculated for each cell type and cellular compartment and this information

738 was represented in the final figure.

739

740 **CAGE Analysis**

741 All available CAGE data from the ENCODE project (Consortium 2012) for 36

742 cell lines was downloaded from the UCSC genome browser (Kent et al. 2002)

743 for genome version hg19. Of these, 28 cell lines had CAGE transcription start

744 sites (TSS) mapping to the plus strand of chromosome 1 and in regions

745 corresponding to 200 base pairs upstream of the *Lnc34a* start site (9241796 -

746 200) and 200 base pairs upstream of the GENCODE annotated *lncTAM34a*

747 start site (9242263 + 200). These cell lines included: HFDPC, H1-hESC,

748 HMEpC, HAoEC, HPIEpC, HSaVEC, GM12878, hMSC-BM, HUVEC,

749 AG04450, hMSC-UC, IMR90, NHDF, SK-N-SH_RA, BJ, HOB, HPC-PL,

750   HAoAF, NHEK, HVMF, HWP, MCF-7, HepG2, hMSC-AT, NHEM.f_M2,

751   SkMC, NHEM_M2, and HCH. In total 74 samples were included. 17 samples

752   were polyA-, 47 samples were polyA+, and 10 samples were total RNA. In

753   addition, 34 samples were whole cell, 15 enriched for the cytosolic fraction, 15

754   enriched for the nucleolus, and 15 enriched for the nucleus. All CAGE

755   transcription start sites were plotted and the RPKM of the individual reads was

756   used to color each read to indicate their relative abundance. In cases where

757   CAGE TSS spanned identical regions, the RPMKs of the regions were

758   summed and represented as one CAGE TSS in the figure. In addition, a

759   density plot shows the distribution of the CAGE reads in the specified

760   interval.

761

762   **Splice Junction Analysis**

763   All available whole cell (i.e. non-fractionated) spliced read data originating

764   from the Cold Spring Harbor Lab in the ENCODE project (Consortium 2012)

765   for 38 cell lines was downloaded from the UCSC genome browser (Kent et al.

766   2002). Of these cell lines, 36 had spliced reads mapping to the plus strand of

767   chromosome 1 and in the region between the *Lnc34a* start (9241796) and

768   transcription termination (9257102) site (note that *lncTAM34a* resides totally

769   within this region). Splice junctions from the following cell lines were included

770   in the final figure: A549, Ag04450, Bj, CD20, CD34 mobilized, Gm12878,

771   H1hesc, Haoaf, Haoec, Hch, Helas3, Hepg2, Hfdpc, Hmec, Hmepc, Hmscat,

772   Hmscbm, Hmscuc, Hob, Hpcpl, Hpiepc, Hsavec, Hsmm, Huvec, Hvmf, Hwp,

773   Imr90, Mcf7, Monocd14, Nhdf, Nhek, Nhemfm2, Nhemm2, Nhlf, Skmc, and

774   Sknsh. All splice junctions were included in the figure and colored according

35

775   to the number of reads corresponding to each. In cases where identical reads

776   were detected multiple times, the read count was summed and represented

777   as one read in the figure.

778

779   **TCGA Data Analysis**

780   RNAseq data and copy number data were downloaded from TCGA and

781   processed as described previously (Ashouri et al. 2016). Briefly, RNAseq data

782   were aligned to the human hg19 assembly and quantified using GENCODE

783   (v19) annotated HTSeq-counts and FPKM normalizations. Expression data

784   from *miR34a* and *lncTAM34a* (identified as RP3-510D11.2) were used for

785   further analysis. Copy number amplitudes for GENCODE genes were

786   determined from segmented copy-number data. Samples that were diploid for

787   *lncTAM34a* were identified as those samples that had copy number

788   amplitudes between -0.1 and 0.1.

789

790   Somatic mutation data were downloaded from the Genomics Data Commons

791   data portal (GDC) as mutation annotation format (maf) files, called using

792   Mutect2 on 30/10/2017 (v7) (Grossman et al. 2016).

793

794   Survival analysis was performed on TCGA vital state and follow-up data,

795   downloaded from GDC on 27/10/2017 using the R survival package

796   (Therneau 2015).

797
798   **Acknowledgments**

801 role in the conceptualization and supervision of this project, sadly passed

802 away before the initial submission of the manuscript. May he rest in peace.

803

Competing Interests

The authors declare no competing interests.

Figure Supplements

Figure 1-Supplement 1: TCAG expression levels and correlation analysis statistics.

Figure 1-Supplement 2: Molecular characteristics of *lncTAM34a*.

Figure 2-Supplement 1: A schematic representation of the p1 construct.

Figure 2-Supplement 2: Evaluating the effects of *lncTAM34a* down-regulation.

Figure 3-Supplement 1: Physiological relevance of *lncTAM34a* over-expression.

Figure 3-Supplement 2: Effects of *lncTAM34a* over-expression on cyclin D1.

Figure 4-Supplement 1: Survival analysis in 17 cancers from TCGA.

Supplementary Document 1: Evaluating the relationship between *lncTAM34a* and *Lnc34a*.

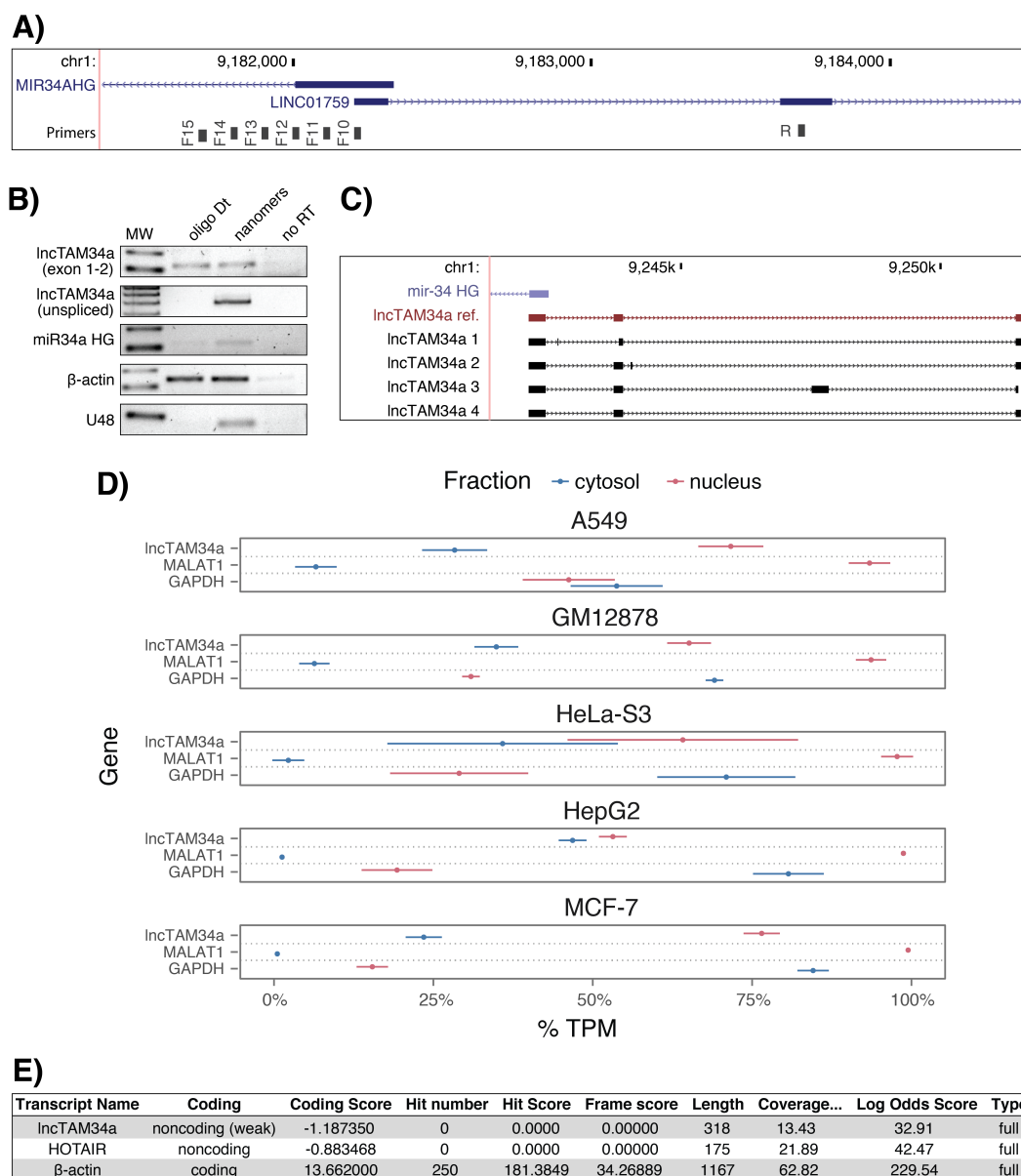Supplementary Document 2: A table of primers used in this study.

Supplementary Figures

A)

| cancer	all n	all rho	all p	TP53wt n	TP53wt rho	TP53wt p	TP53mut n	TP53mut rho	TP53mut p
Adrenocortical carcinoma (ACC)	10	0.55	1.04e−01	10	0.55	1.04e−01	NA	NA	NA
Bladder Urothelial Carcinoma (BLCA)	228	0.51	7.89e−17	134	0.45	3.86e−08	94	0.43	1.73e−05
Breast invasive carcinoma (BRCA) Basal	42	0.57	9.54e−05	10	0.62	6.02e−02	32	0.57	7.41e−04
Breast invasive carcinoma (BRCA) Her2	44	0.15	3.39e−01	12	0.22	4.85e−01	32	0.07	7.10e−01
Breast invasive carcinoma (BRCA) LumA	199	0.34	8.22e−07	177	0.34	2.96e−06	22	0.49	2.31e−02
Breast invasive carcinoma (BRCA) LumB	70	0.17	1.57e−01	61	0.15	2.53e−01	9	0.17	6.78e−01
Cervical squamous cell carcinoma and endocervical adenocarcinoma (CESC)	156	0.14	8.37e−02	145	0.16	5.45e−02	11	−0.05	9.03e−01
Head and Neck squamous cell carcinoma (HNSC)	313	0.54	8.38e−25	123	0.61	0.00e+00	190	0.45	9.68e−11
Kidney Chromophobe (KICH)	5	0.60	3.50e−01	5	0.60	3.50e−01	NA	NA	NA
Kidney renal clear cell carcinoma (KIRC)	142	0.35	2.06e−05	141	0.34	4.41e−05	NA	NA	NA
Kidney renal papillary cell carcinoma (KIRP)	167	0.45	9.16e−10	163	0.45	2.04e−09	4	0.80	3.33e−01
Brain Lower Grade Glioma (LGG)	271	0.63	9.92e−32	76	0.73	0.00e+00	195	0.39	2.26e−08
Liver hepatocellular carcinoma (LIHC)	153	0.56	3.64e−14	114	0.52	4.18e−09	39	0.45	3.95e−03
Lung adenocarcinoma (LUAD)	234	0.28	1.15e−05	128	0.36	2.87e−05	106	0.23	1.91e−02
Lung squamous cell carcinoma (LUSC)	139	0.23	6.74e−03	42	0.04	7.93e−01	97	0.33	9.91e−04
Ovarian serous cystadenocarcinoma (OV)	56	0.23	8.37e−02	10	0.84	4.46e−03	46	0.15	3.31e−01
Prostate adenocarcinoma (PRAD)	413	0.47	1.33e−23	375	0.46	6.13e−21	38	0.45	4.58e−03
Skin Cutaneous Melanoma (SKCM)	165	0.65	5.43e−21	152	0.61	7.85e−17	13	0.43	1.40e−01
Stomach adenocarcinoma (STAD)	225	0.37	8.23e−09	145	0.37	5.71e−06	80	0.42	1.03e−04
Thyroid carcinoma (THCA)	469	0.46	1.07e−25	467	0.46	4.06e−26	NA	NA	NA

B)
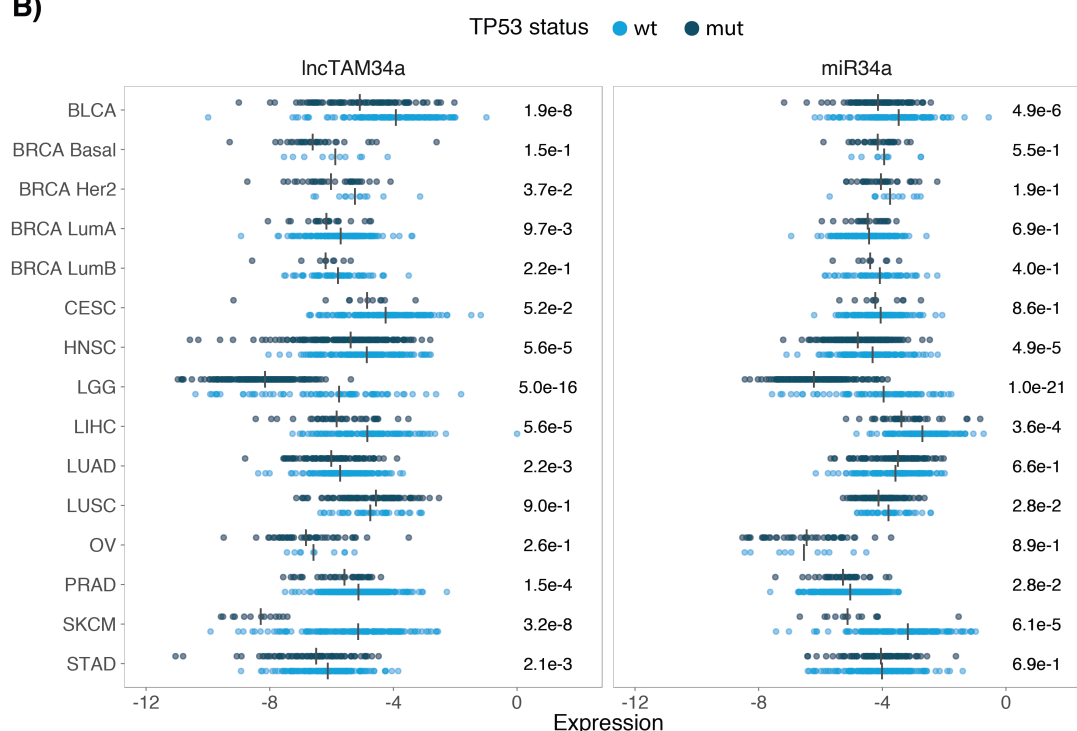
Figure 1 Supplement 1: TCGA normalized expression levels and correlation analysis statistics. **A)** Spearman's rho and *P* values (p) from the correlation analysis in Figure 1a between *miR34a* and *lncTAM34a* expression in *TP53* wild type (wt) and mutated (mut) samples within TCGA cancer types. NA indicates not applicable, due to a lack of data for the specific group. **B)** Expression levels of *miR34a* and *lncTAM34a* in *TP53* wt and nonsynonymous mutation samples. Expression was quantified by the log2 ratio of expression of the gene to its maximal expression value. Vertical lines indicate the median. *P* values are indicated on the right side of each panel and are derived from comparing the *TP53* wild type samples to the samples with a nonsynonymous mutation using a two-sided Wilcoxon signed rank test. Only cancers that had at least 5 samples per group were included. In addition, only samples that were diploid at the *miR34a* locus were used for the analysis to avoid copy number bias.

Transcript Name	Coding	Coding Score	Hit number	Hit Score	Frame score	Length	Coverage...	Log Odds Score	Type
lncTAM34a	noncoding (weak)	-1.187350	0	0.0000	0.00000	318	13.43	32.91	full
HOTAIR	noncoding	-0.883468	0	0.0000	0.00000	175	21.89	42.47	full
β-actin	coding	13.662000	250	181.3849	34.26889	1167	62.82	229.54	full

852
853
854 **Figure 1 Supplement 2: Molecular characteristics of *lncTAM34a*. A)** A schematic representation of
855 the primer placement in the primer walk assay. **B)** Polyadenylation status of spliced and
856 unspliced *lncTAM34a* in HEK293T cells. **C)** Sequencing results from the analysis of *lncTAM34a*
857 isoforms in U2OS cells. *lncTAM34a* ref. refers to the full-length transcript as defined by the 3'-RACE
858 and the primer walk assay. **D)** Analysis of coding potential of the *lncTAM34a* transcript using the
859 Coding-potential Calculator. **E)** RNAseq data from five fractionated cell lines in the ENCODE project
860 showing the percentage of transcripts per million (TPM) for *lncTAM34a*. *MALAT1* (nuclear
861 localization) and *GAPDH* (cytoplasmic localization) are included as fractionation controls. Points
862 represent the mean and horizontal lines represent the standard deviation from two biological replicates.
863

39
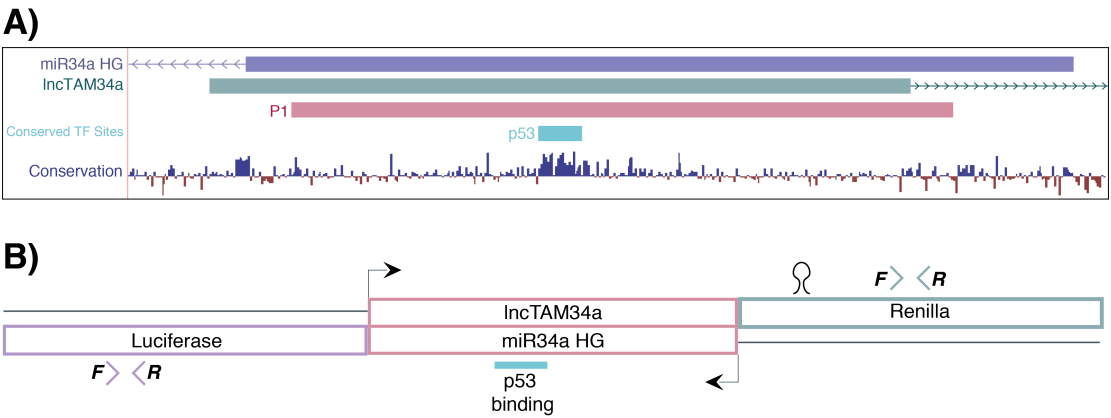
Figure 2 Supplement 1: A schematic representation of the p1 construct. A) A UCSC genome browser illustration indicating the location of the promoter region cloned into the p1 construct including the conserved TP53-binding site. **B)** A representative picture of the p1 construct including forward (F) and reverse (R) primer locations and the renilla shRNA targeting site.
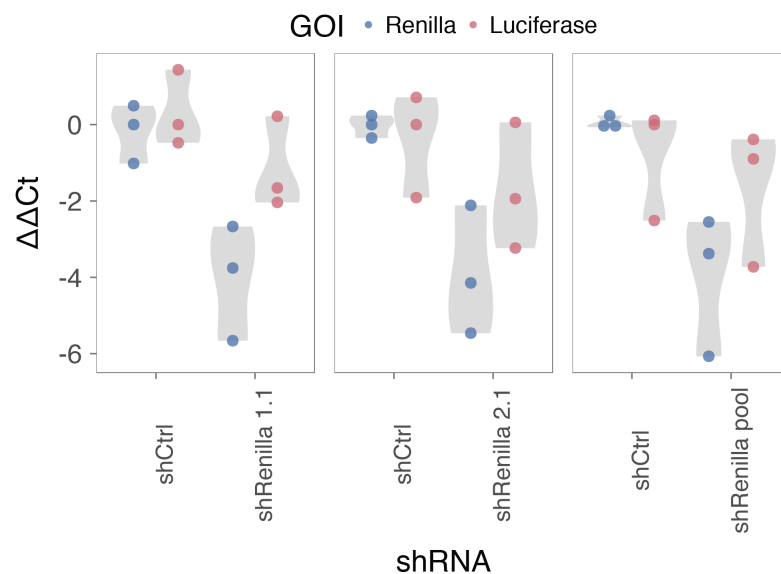
Figure 2 Supplement 2: Evaluating the effects of *lncTAM34a* down-regulation. HEK293T cells were co-transfected with the p1 construct and either shRenilla or shControl. Renilla and luciferase levels were measured with QPCR 48 hours after transfection. Individual points represent independent experiments with the gray shadow indicating the density of the points. The experiment was performed in biological triplicate.
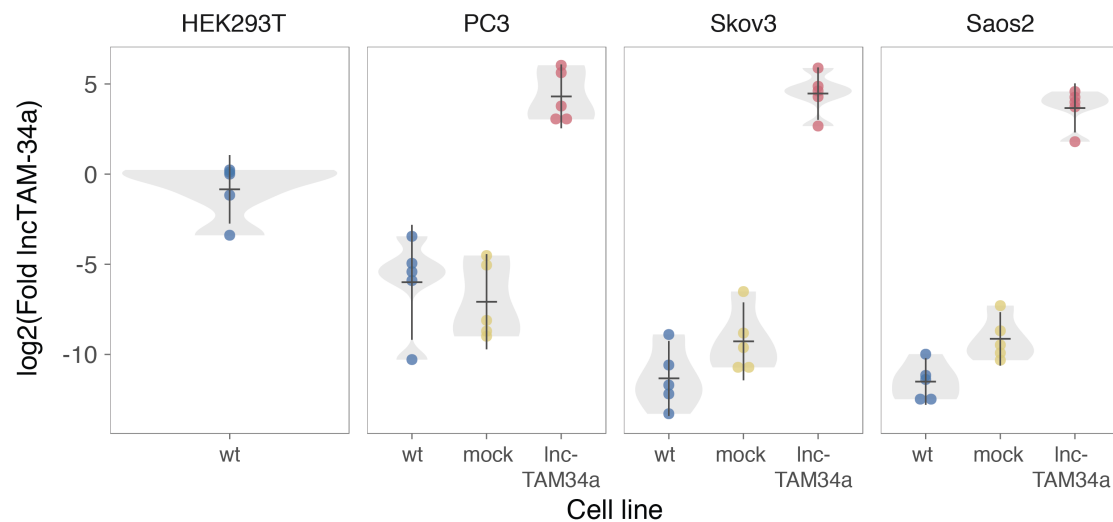
Figure 3 Supplement 1: Physiological relevance of *lncTAM34a* over-expression. Comparison of *lncTAM34a* expression in HEK293T cells (high endogenous *lncTAM34a*), and the wild-type (wt), mock, and *lncTAM34a* over-expressing stable cell lines.
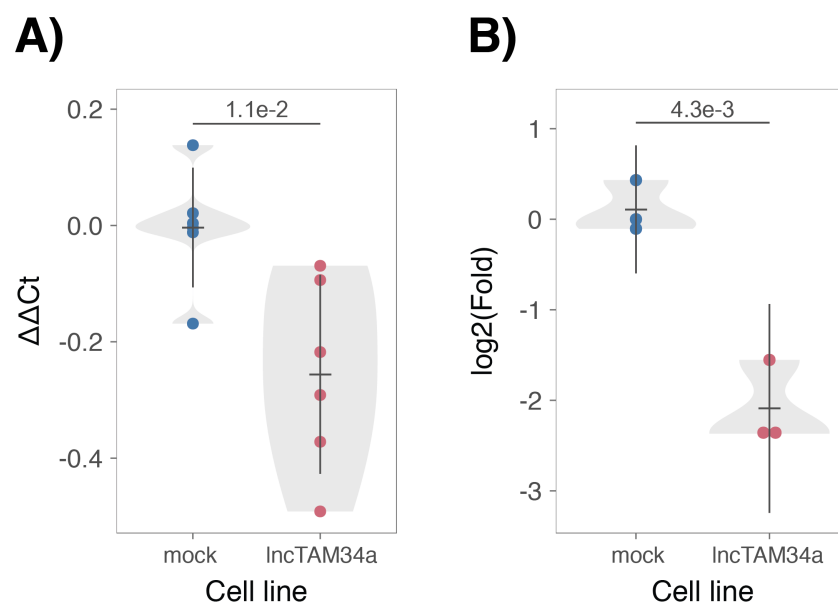
Figure 3 Supplement 2: Effects of *lncTAM34a* over-expression on cyclin D1. CCND1 expression **(A)** and western blot quantification of protein levels **(B)** in *lncTAM34a* over-expressing PC3 stable cell lines. Experiments were performed in biological sextuplets **(A)** or triplicates **(B)**.

43
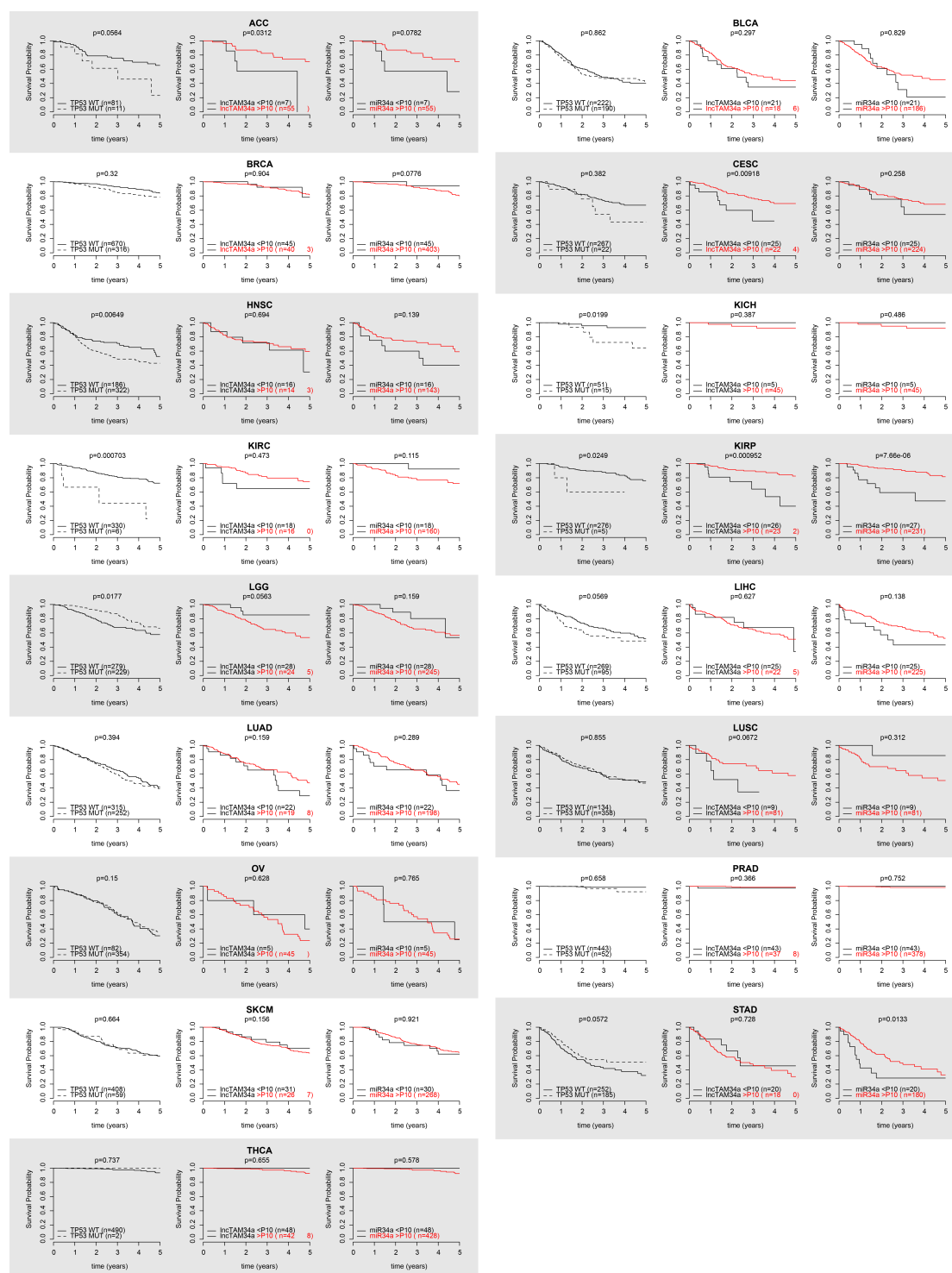
— TP53 WT   - - TP53 MUT   — Low expression (<P10)   — Normal expression (>P10)

Figure 4-Supplement 1: Survival analysis in 17 cancers from TCGA. Kaplan-Meier survival curves comparing the survival of *TP53*-mutated samples (left), low *lncTAM34a* expression (middle) and low *miR34a* expression (right) to control samples in 17 cancer types from TCGA. Low expression was defined as *TP53* non-mutated samples having expression values in the bottom 10th percentile.

44

893
References
895

896 Agostini, M., P. Tucci, R. Killick, E. Candi, B. S. Sayan, P. Rivetti di Val Cervo, P.
897 Nicotera, F. McKeon, R. A. Knight, T. W. Mak and G. Melino (2011). "Neuronal
898 differentiation by TAp73 is mediated by microRNA-34a regulation of synaptic
899 protein targets." Proc Natl Acad Sci U S A **108**(52): 21093-21098. DOI:
900 10.1073/pnas.1112061109

902 Ahn, Y. H., D. L. Gibbons, D. Chakravarti, C. J. Creighton, Z. H. Rizvi, H. P. Adams, A.
903 Pertsemlidis, P. A. Gregory, J. A. Wright, G. J. Goodall, E. R. Flores and J. M. Kurie
904 (2012). "ZEB1 drives prometastatic actin cytoskeletal remodeling by
905 downregulating miR-34a expression." J Clin Invest **122**(9): 3170-3183. DOI:
906 10.1172/JCI63608

908 Allaire, J., Y. Xie, J. McPherson, J. Luraschi, K. Ushey, A. Atkins, H. Wickham, J.
909 Cheng and W. Chang (2017). rmarkdown: Dynamic Documents for R. R package
910 version 1.8. https://CRAN.R-project.org/package=rmarkdown

912 Amarzguioui, M., J. J. Rossi and D. Kim (2005). "Approaches for chemically
913 synthesized siRNA and vector-mediated RNAi." FEBS Lett **579**(26): 5974-5981.
914 DOI: 10.1016/j.febslet.2005.08.070

916 Arnold, J. B. (2017). ggthemes: Extra Themes, Scales and Geoms for 'ggplot2'. R
917 package version 3.4.0. https://CRAN.R-project.org/package=ggthemes

919 Ashouri, A., V. I. Sayin, J. Van den Eynden, S. X. Singh, T. Papagiannakopoulos and
920 E. Larsson (2016). "Pan-cancer transcriptomic analysis associates long non-
921 coding RNAs with key mutational driver events." Nature Communications **7**:
922 13197. DOI: 10.1038/ncomms13197

924 Balbin, O. A., R. Malik, S. M. Dhanasekaran, J. R. Prensner, X. Cao, Y. M. Wu, D.
925 Robinson, R. Wang, G. Chen, D. G. Beer, A. I. Nesvizhskii and A. M. Chinnaiyan
926 (2015). "The landscape of antisense gene expression in human cancers." Genome
927 Res **25**(7): 1068-1079. DOI: 10.1101/gr.180596.114

929 Boekel, J., J. M. Chilton, I. R. Cooke, P. L. Horvatovich, P. D. Jagtap, L. Kall, J. Lehtio,
930 P. Lukasse, P. D. Moerland and T. J. Griffin (2015). "Multi-omic data analysis using
931 Galaxy." Nat Biotechnol **33**(2): 137-139. DOI: 10.1038/nbt.3134

933 Boque-Sastre, R., M. Soler, C. Oliveira-Mateos, A. Portela, C. Moutinho, S. Sayols, A.
934 Villanueva, M. Esteller and S. Guil (2015). "Head-to-head antisense transcription
935 and R-loop formation promotes transcriptional activation." Proc Natl Acad Sci U
936 S A **112**(18): 5785-5790. DOI: 10.1073/pnas.1421197112

938 Chang, T. C., D. Yu, Y. S. Lee, E. A. Wentzel, D. E. Arking, K. M. West, C. V. Dang, A.
939 Thomas-Tikhonenko and J. T. Mendell (2008). "Widespread microRNA
940 repression by Myc contributes to tumorigenesis." Nat Genet **40**(1): 43-50. DOI:
941 10.1038/ng.2007.30

942

943   Chang, W. (2014). extrafont: Tools for using fonts. R package version 0.17.
944   https://CRAN.R-project.org/package=extrafont

945

946   Chen, J., M. Sun, W. J. Kent, X. Huang, H. Xie, W. Wang, G. Zhou, R. Z. Shi and J. D.
947   Rowley (2004). "Over 20% of human transcripts might form sense-antisense
948   pairs." Nucleic Acids Res **32**(16): 4812-4820. DOI: 10.1093/nar/gkh818

949

950   Cheng, J., L. Zhou, Q. F. Xie, H. Y. Xie, X. Y. Wei, F. Gao, C. Y. Xing, X. Xu, L. J. Li and S.
951   S. Zheng (2010). "The impact of miR-34a on protein output in hepatocellular
952   carcinoma HepG2 cells." Proteomics **10**(8): 1557-1572. DOI:
953   10.1002/pmic.200900646

954

955   Chim, C. S., K. Y. Wong, Y. Qi, F. Loong, W. L. Lam, L. G. Wong, D. Y. Jin, J. F. Costello
956   and R. Liang (2010). "Epigenetic inactivation of the miR-34a in hematological
957   malignancies." Carcinogenesis **31**(4): 745-750. DOI: 10.1093/carcin/bgq033

958

959   Cole, K. A., E. F. Attiyeh, Y. P. Mosse, M. J. Laquaglia, S. J. Diskin, G. M. Brodeur and
960   J. M. Maris (2008). "A functional screen identifies miR-34a as a candidate
961   neuroblastoma tumor suppressor gene." Mol Cancer Res **6**(5): 735-742. DOI:
962   10.1158/1541-7786.MCR-07-2102

963

964   Conley, A. B. and I. K. Jordan (2012). "Epigenetic regulation of human cis-natural
965   antisense transcripts." Nucleic Acids Res **40**(4): 1438-1445. DOI:
966   10.1093/nar/gkr1010

967

968   Encode Project Consortium (2012). "An integrated encyclopedia of DNA
969   elements in the human genome." Nature **489**(7414): 57-74. DOI:
970   10.1038/nature11247

971

972   Ding, N., H. Wu, T. Tao and E. Peng (2017). "NEAT1 regulates cell proliferation
973   and apoptosis of ovarian cancer by miR-34a-5p/BCL2." Onco Targets Ther **10**:
974   4905-4915. DOI: 10.2147/OTT.S142446

975

976   Djebali, S., C. A. Davis, A. Merkel, A. Dobin, T. Lassmann, A. Mortazavi, A. Tanzer, J.
977   Lagarde, W. Lin, F. Schlesinger, C. Xue, G. K. Marinov, J. Khatun, B. A. Williams, C.
978   Zaleski, J. Rozowsky, M. Roder, F. Kokocinski, R. F. Abdelhamid, T. Alioto, I.
979   Antoshechkin, M. T. Baer, N. S. Bar, P. Batut, K. Bell, I. Bell, S. Chakrabortty, X.
980   Chen, J. Chrast, J. Curado, T. Derrien, J. Drenkow, E. Dumais, J. Dumais, R.
981   Duttagupta, E. Falconnet, M. Fastuca, K. Fejes-Toth, P. Ferreira, S. Foissac, M. J.
982   Fullwood, H. Gao, D. Gonzalez, A. Gordon, H. Gunawardena, C. Howald, S. Jha, R.
983   Johnson, P. Kapranov, B. King, C. Kingswood, O. J. Luo, E. Park, K. Persaud, J. B.
984   Preall, P. Ribeca, B. Risk, D. Robyr, M. Sammeth, L. Schaffer, L. H. See, A. Shahab, J.
985   Skancke, A. M. Suzuki, H. Takahashi, H. Tilgner, D. Trout, N. Walters, H. Wang, J.
986   Wrobel, Y. Yu, X. Ruan, Y. Hayashizaki, J. Harrow, M. Gerstein, T. Hubbard, A.
987   Reymond, S. E. Antonarakis, G. Hannon, M. C. Giddings, Y. Ruan, B. Wold, P.
988   Carninci, R. Guigo and T. R. Gingeras (2012). "Landscape of transcription in
989   human cells." Nature **489**(7414): 101-108. DOI: 10.1038/nature11233

990

991 Gallardo, E., A. Navarro, N. Vinolas, R. M. Marrades, T. Diaz, B. Gel, A. Quera, E.
992 Bandres, J. Garcia-Foncillas, J. Ramirez and M. Monzo (2009). "miR-34a as a
993 prognostic marker of relapse in surgically resected non-small-cell lung cancer."
994 Carcinogenesis **30**(11): 1903-1909. DOI: 10.1093/carcin/bgp219
995
996 Geiger, T., A. Wehner, C. Schaab, J. Cox and M. Mann (2012). "Comparative
997 proteomic analysis of eleven common cell lines reveals ubiquitous but varying
998 expression of most proteins." Mol Cell Proteomics **11**(3): M111 014050. DOI:
999 10.1074/mcp.M111.014050
1000
1001 Granholm, V., S. Kim, J. C. Navarro, E. Sjolund, R. D. Smith and L. Kall (2014). "Fast
1002 and accurate database searches with MS-GF+Percolator." J Proteome Res **13**(2):
1003 890-897. DOI: 10.1021/pr400937n
1004
1005 Grossman, R. L., A. P. Heath, V. Ferretti, H. E. Varmus, D. R. Lowy, W. A. Kibbe and
1006 L. M. Staudt (2016). "Toward a Shared Vision for Cancer Genomic Data." N Engl J
1007 Med **375**(12): 1109-1112. DOI: 10.1056/NEJMp1607591
1008
1009 Holman, J. D., D. L. Tabb and P. Mallick (2014). "Employing ProteoWizard to
1010 Convert Raw Mass Spectrometry Data." Curr Protoc Bioinformatics **46**: 13 24 11-
1011 19. DOI: 10.1002/0471250953.bi1324s46
1012
1013 Hung, T., Y. Wang, M. F. Lin, A. K. Koegel, Y. Kotake, G. D. Grant, H. M. Horlings, N.
1014 Shah, C. Umbricht, P. Wang, Y. Wang, B. Kong, A. Langerod, A. L. Borresen-Dale, S.
1015 K. Kim, M. van de Vijver, S. Sukumar, M. L. Whitfield, M. Kellis, Y. Xiong, D. J. Wong
1016 and H. Y. Chang (2011). "Extensive and coordinated transcription of noncoding
1017 RNAs within cell-cycle promoters." Nat Genet **43**(7): 621-629. DOI:
1018 10.1038/ng.848
1019
1020 Hunten, S., M. Kaller, F. Drepper, S. Oeljeklaus, T. Bonfert, F. Erhard, A. Dueck, N.
1021 Eichner, C. C. Friedel, G. Meister, R. Zimmer, B. Warscheid and H. Hermeking
1022 (2015). "p53-Regulated Networks of Protein, mRNA, miRNA, and lncRNA
1023 Expression Revealed by Integrated Pulsed Stable Isotope Labeling With Amino
1024 Acids in Cell Culture (pSILAC) and Next Generation Sequencing (NGS) Analyses."
1025 Mol Cell Proteomics **14**(10): 2609-2629. DOI: 10.1074/mcp.M115.050237
1026
1027 International Human Genome Sequencing Consortium. (2004). "Finishing the
1028 euchromatic sequence of the human genome." Nature **431**(7011): 931-945. DOI:
1029 10.1038/nature03001
1030
1031 Johnsson, P., A. Ackley, L. Vidarsdottir, W. O. Lui, M. Corcoran, D. Grander and K.
1032 V. Morris (2013). "A pseudogene long-noncoding-RNA network regulates PTEN
1033 transcription and translation in human cells." Nat Struct Mol Biol **20**(4): 440-
1034 446. DOI: 10.1038/nsmb.2516
1035
1036 Katayama, S., Y. Tomaru, T. Kasukawa, K. Waki, M. Nakanishi, M. Nakamura, H.
1037 Nishida, C. C. Yap, M. Suzuki, J. Kawai, H. Suzuki, P. Carninci, Y. Hayashizaki, C.
1038 Wells, M. Frith, T. Ravasi, K. C. Pang, J. Hallinan, J. Mattick, D. A. Hume, L. Lipovich,
1039 S. Batalov, P. G. Engstrom, Y. Mizuno, M. A. Faghihi, A. Sandelin, A. M. Chalk, S.

Mottagui-Tabar, Z. Liang, B. Lenhard, C. Wahlestedt, R. G. E. R. Group, G. Genome Science and F. Consortium (2005). "Antisense transcription in the mammalian transcriptome." Science **309**(5740): 1564-1566. DOI: 10.1126/science.1112009

Kent, W. J., C. W. Sugnet, T. S. Furey, K. M. Roskin, T. H. Pringle, A. M. Zahler and D. Haussler (2002). "The human genome browser at UCSC." Genome Res **12**(6): 996-1006. DOI: 10.1101/gr.229102. Article published online before print in May 2002

Kim, K. H., H. J. Kim and T. R. Lee (2017). "Epidermal long non-coding RNAs are regulated by ultraviolet irradiation." Gene **637**: 196-202. DOI: 10.1016/j.gene.2017.09.043

Kim, S. and P. A. Pevzner (2014). "MS-GF+ makes progress towards a universal database search tool for proteomics." Nature Communications **5**: 5277. DOI: 10.1038/ncomms6277

Kong, L., Y. Zhang, Z. Q. Ye, X. Q. Liu, S. Q. Zhao, L. Wei and G. Gao (2007). "CPC: assess the protein-coding potential of transcripts using sequence features and support vector machine." Nucleic Acids Res **35**(Web Server issue): W345-349. DOI: 10.1093/nar/gkm391

Lal, A., M. P. Thomas, G. Altschuler, F. Navarro, E. O'Day, X. L. Li, C. Concepcion, Y. C. Han, J. Thiery, D. K. Rajani, A. Deutsch, O. Hofmann, A. Ventura, W. Hide and J. Lieberman (2011). "Capture of microRNA-bound mRNAs identifies the tumor suppressor miR-34a as a regulator of growth factor signaling." PLoS Genet **7**(11): e1002363. DOI: 10.1371/journal.pgen.1002363

Leveille, N., C. A. Melo, K. Rooijers, A. Diaz-Lagares, S. A. Melo, G. Korkmaz, R. Lopes, F. Akbari Moqadam, A. R. Maia, P. J. Wijchers, G. Geeven, M. L. den Boer, R. Kalluri, W. de Laat, M. Esteller and R. Agami (2015). "Genome-wide profiling of p53-regulated enhancer RNAs uncovers a subset of enhancers controlled by a lncRNA." Nature Communications **6**: 6520. DOI: 10.1038/ncomms7520

Liu, C., K. Kelnar, B. Liu, X. Chen, T. Calhoun-Davis, H. Li, L. Patrawala, H. Yan, C. Jeter, S. Honorio, J. F. Wiggins, A. G. Bader, R. Fagin, D. Brown and D. G. Tang (2011). "The microRNA miR-34a inhibits prostate cancer stem cells and metastasis by directly repressing CD44." Nat Med **17**(2): 211-215. DOI: 10.1038/nm.2284

Memczak, S., M. Jens, A. Elefsinioti, F. Torti, J. Krueger, A. Rybak, L. Maier, S. D. Mackowiak, L. H. Gregersen, M. Munschauer, A. Loewer, U. Ziebold, M. Landthaler, C. Kocks, F. le Noble and N. Rajewsky (2013). "Circular RNAs are a large class of animal RNAs with regulatory potency." Nature **495**(7441): 333-338. DOI: 10.1038/nature11928

Ng, S. Y., G. K. Bogu, B. S. Soh and L. W. Stanton (2013). "The long noncoding RNA RMST interacts with SOX2 to regulate neurogenesis." Mol Cell **51**(3): 349-359. DOI: 10.1016/j.molcel.2013.07.017

1089
1090 Ng, S. Y., R. Johnson and L. W. Stanton (2012). "Human long non-coding RNAs
1091 promote pluripotency and neuronal differentiation by association with
1092 chromatin modifiers and transcription factors." EMBO J **31**(3): 522-533. DOI:
1093 10.1038/emboj.2011.459
1094
1095 O'Leary, N. A., M. W. Wright, J. R. Brister, S. Ciufo, D. Haddad, R. McVeigh, B.
1096 Rajput, B. Robbertse, B. Smith-White, D. Ako-Adjei, A. Astashyn, A. Badretdin, Y.
1097 Bao, O. Blinkova, V. Brover, V. Chetvernin, J. Choi, E. Cox, O. Ermolaeva, C. M.
1098 Farrell, T. Goldfarb, T. Gupta, D. Haft, E. Hatcher, W. Hlavina, V. S. Joardar, V. K.
1099 Kodali, W. Li, D. Maglott, P. Masterson, K. M. McGarvey, M. R. Murphy, K. O'Neill,
1100 S. Pujar, S. H. Rangwala, D. Rausch, L. D. Riddick, C. Schoch, A. Shkeda, S. S. Storz,
1101 H. Sun, F. Thibaud-Nissen, I. Tolstoy, R. E. Tully, A. R. Vatsan, C. Wallin, D. Webb,
1102 W. Wu, M. J. Landrum, A. Kimchi, T. Tatusova, M. DiCuccio, P. Kitts, T. D. Murphy
1103 and K. D. Pruitt (2016). "Reference sequence (RefSeq) database at NCBI: current
1104 status, taxonomic expansion, and functional annotation." Nucleic Acids Res
1105 **44**(D1): D733-745. DOI: 10.1093/nar/gkv1189
1106
1107 Ozsolak, F., P. Kapranov, S. Foissac, S. W. Kim, E. Fishilevich, A. P. Monaghan, B.
1108 John and P. M. Milos (2010). "Comprehensive polyadenylation site maps in yeast
1109 and human reveal pervasive alternative polyadenylation." Cell **143**(6): 1018-
1110 1029. DOI: 10.1016/j.cell.2010.11.020
1111
1112 Polson, A., E. Durrett and D. Reisman (2011). "A bidirectional promoter reporter
1113 vector for the analysis of the p53/WDR79 dual regulatory element." Plasmid
1114 **66**(3): 169-179. DOI: 10.1016/j.plasmid.2011.08.004
1115
1116 Rashi-Elkeles, S., H. J. Warnatz, R. Elkon, A. Kupershtein, Y. Chobod, A. Paz, V.
1117 Amstislavskiy, M. Sultan, H. Safer, W. Nietfeld, H. Lehrach, R. Shamir, M. L. Yaspo
1118 and Y. Shiloh (2014). "Parallel profiling of the transcriptome, cistrome, and
1119 epigenome in the cellular response to ionizing radiation." Sci Signal **7**(325): rs3.
1120 DOI: 10.1126/scisignal.2005032
1121
1122 Raver-Shapira, N., E. Marciano, E. Meiri, Y. Spector, N. Rosenfeld, N. Moskovits, Z.
1123 Bentwich and M. Oren (2007). "Transcriptional activation of miR-34a
1124 contributes to p53-mediated apoptosis." Mol Cell **26**(5): 731-743. DOI:
1125 10.1016/j.molcel.2007.05.017
1126
1127 Rinn, J. L., M. Kertesz, J. K. Wang, S. L. Squazzo, X. Xu, S. A. Brugmann, L. H.
1128 Goodnough, J. A. Helms, P. J. Farnham, E. Segal and H. Y. Chang (2007).
1129 "Functional demarcation of active and silent chromatin domains in human HOX
1130 loci by noncoding RNAs." Cell **129**(7): 1311-1323. DOI:
1131 10.1016/j.cell.2007.05.022
1132
1133 Rokavec, M., M. G. Oner, H. Li, R. Jackstadt, L. Jiang, D. Lodygin, M. Kaller, D. Horst,
1134 P. K. Ziegler, S. Schwitalla, J. Slotta-Huspenina, F. G. Bader, F. R. Greten and H.
1135 Hermeking (2015). "Corrigendum. IL-6R/STAT3/miR-34a feedback loop
1136 promotes EMT-mediated colorectal cancer invasion and metastasis." J Clin Invest
1137 **125**(3): 1362. DOI: 10.1172/JCI81340

1138
1139 Schneider, C. A., W. S. Rasband and K. W. Eliceiri (2012). "NIH Image to ImageJ:
1140 25 years of image analysis." Nat Methods **9**(7): 671-675.
1141
1142 Serviss, J. T. (2017). miR34AasRNAproject.
1143 https://github.com/GranderLab/miR34a_asRNA_project
1144
1145 Serviss, J. T., P. Johnsson and D. Grander (2014). "An emerging role for long non-
1146 coding RNAs in cancer metastasis." Front Genet **5**: 234. DOI:
1147 10.3389/fgene.2014.00234
1148
1149 Slabakova, E., Z. Culig, J. Remsik and K. Soucek (2017). "Alternative mechanisms
1150 of miR-34a regulation in cancer." Cell Death Dis **8**(10): e3100. DOI:
1151 10.1038/cddis.2017.495
1152
1153 Stahlhut, C. and F. J. Slack (2015). "Combinatorial Action of MicroRNAs let-7 and
1154 miR-34 Effectively Synergizes with Erlotinib to Suppress Non-small Cell Lung
1155 Cancer Cell Proliferation." Cell Cycle **14**(13): 2171-2180. DOI:
1156 10.1080/15384101.2014.1003008
1157
1158 Su, X., D. Chakravarti, M. S. Cho, L. Liu, Y. J. Gi, Y. L. Lin, M. L. Leung, A. El-Naggar,
1159 C. J. Creighton, M. B. Suraokar, I. Wistuba and E. R. Flores (2010). "TAp63
1160 suppresses metastasis through coordinate regulation of Dicer and miRNAs."
1161 Nature **467**(7318): 986-990. DOI: 10.1038/nature09459
1162
1163 Sun, F., H. Fu, Q. Liu, Y. Tie, J. Zhu, R. Xing, Z. Sun and X. Zheng (2008).
1164 "Downregulation of CCND1 and CDK6 by miR-34a induces cell cycle arrest."
1165 FEBS Lett **582**(10): 1564-1568. DOI: 10.1016/j.febslet.2008.03.057
1166
1167 Tarasov, V., P. Jung, B. Verdoodt, D. Lodygin, A. Epanchintsev, A. Menssen, G.
1168 Meister and H. Hermeking (2007). "Differential regulation of microRNAs by p53
1169 revealed by massively parallel sequencing: miR-34a is a p53 target that induces
1170 apoptosis and G1-arrest." Cell Cycle **6**(13): 1586-1593. DOI:
1171 10.4161/cc.6.13.4436
1172
1173 Team, R. C. (2017). "R: A Language and Environment for Statistical Computing."
1174 from https://www.R-project.org/.
1175
1176 Therneau, T. M. (2015). A Package for Survival Analysis in S. version 2.38.
1177 https://CRAN.R-project.org/package=survival
1178
1179 Turner, A. M., A. M. Ackley, M. A. Matrone and K. V. Morris (2012).
1180 "Characterization of an HIV-targeted transcriptional gene-silencing RNA in
1181 primary cells." Hum Gene Ther **23**(5): 473-483. DOI: 10.1089/hum.2011.165
1182
1183 Vogt, M., J. Munding, M. Gruner, S. T. Liffers, B. Verdoodt, J. Hauk, L.
1184 Steinstraesser, A. Tannapfel and H. Hermeking (2011). "Frequent concomitant
1185 inactivation of miR-34a and miR-34b/c by CpG methylation in colorectal,
1186 pancreatic, mammary, ovarian, urothelial, and renal cell carcinomas and soft

tissue sarcomas." Virchows Arch **458**(3): 313-322. DOI: 10.1007/s00428-010-1030-5

Wang, L., P. Bu, Y. Ai, T. Srinivasan, H. J. Chen, K. Xiang, S. M. Lipkin and X. Shen (2016). "A long non-coding RNA targets microRNA miR-34a to regulate colon cancer stem cell asymmetric division." Elife **5**. DOI: 10.7554/eLife.14620

Wang, L., H. J. Park, S. Dasari, S. Wang, J. P. Kocher and W. Li (2013). "CPAT: Coding-Potential Assessment Tool using an alignment-free logistic regression model." Nucleic Acids Res **41**(6): e74. DOI: 10.1093/nar/gkt006

Wang, X., J. Li, K. Dong, F. Lin, M. Long, Y. Ouyang, J. Wei, X. Chen, Y. Weng, T. He and H. Zhang (2015). "Tumor suppressor miR-34a targets PD-L1 and functions as a potential immunotherapeutic target in acute myeloid leukemia." Cell Signal **27**(3): 443-452. DOI: 10.1016/j.cellsig.2014.12.003

Wickham, H. (2016). gtable: Arrange 'Grobs' in Tables. R package version 0.2.0. https://CRAN.R-project.org/package=gtable

Wickham, H. (2017). scales: Scale Functions for Visualization. R package version 0.5.0. https://CRAN.R-project.org/package=scales

Wickham, H. (2017). tidyverse: Easily Install and Load the 'Tidyverse'. R package version 1.2.1. https://CRAN.R-project.org/package=tidyverse

Wickham, L. H. a. H. (2017). rlang: Functions for Base Types and Core R and 'Tidyverse' Features. R package version 0.1.4. https://CRAN.R-project.org/package=rlang

Wickham, S. M. B. a. H. (2014). magrittr: A Forward-Pipe Operator for R. R package version 1.5. https://CRAN.R-project.org/package=magrittr

Wilkins, D. gggenes: Draw Gene Arrow Maps in 'ggplot2'. R package version 0.2.0.9003. https://github.com/wilkox/gggenes

Xiao, N. (2017). liftr: Containerize R Markdown Documents. R package version 0.7. https://CRAN.R-project.org/package=liftr

Xie, Y. (2017). knitr: A General-Purpose Package for Dynamic Report Generation in R. R package version 1.17. https://yihui.name/knitr/

Yang, P., Q. J. Li, Y. Feng, Y. Zhang, G. J. Markowitz, S. Ning, Y. Deng, J. Zhao, S. Jiang, Y. Yuan, H. Y. Wang, S. Q. Cheng, D. Xie and X. F. Wang (2012). "TGF-beta-miR-34a-CCL22 signaling-induced Treg cell recruitment promotes venous metastases of HBV-positive hepatocellular carcinoma." Cancer Cell **22**(3): 291-303. DOI: 10.1016/j.ccr.2012.07.023

Yap, K. L., S. Li, A. M. Munoz-Cabello, S. Raguz, L. Zeng, S. Mujtaba, J. Gil, M. J. Walsh and M. M. Zhou (2010). "Molecular interplay of the noncoding RNA ANRIL

1236 and methylated histone H3 lysine 27 by polycomb CBX7 in transcriptional
1237 silencing of INK4a." Mol Cell **38**(5): 662-674. DOI: 10.1016/j.molcel.2010.03.021
1238
1239 Yu, W., D. Gius, P. Onyango, K. Muldoon-Jacobs, J. Karp, A. P. Feinberg and H. Cui
1240 (2008). "Epigenetic silencing of tumour suppressor gene p15 by its antisense
1241 RNA." Nature **451**(7175): 202-206. DOI: 10.1038/nature06468
1242
1243 Zenz, T., J. Mohr, E. Eldering, A. P. Kater, A. Buhler, D. Kienle, D. Winkler, J. Durig,
1244 M. H. van Oers, D. Mertens, H. Dohner and S. Stilgenbauer (2009). "miR-34a as
1245 part of the resistance network in chronic lymphocytic leukemia." Blood **113**(16):
1246 3801-3808. DOI: 10.1182/blood-2008-08-172254
1247
1248